RESEARCH ARTICLE

Key Points:
- St. Anna Trough outflow shows warm, saline, and dense fraction associated with Atlantic Water
- A year-long mooring data suggest density-driven component of the St. Anna Trough flow
- Modeling confirms that the cross-slope density gradient affects the St. Anna Trough flow

Correspondence to:
I. A. Dmitrenko,
igor.dmitrenko@umanitoba.ca

Atlantic water flow into the Arctic Ocean through the St. Anna Trough in the northern Kara Sea

Igor A. Dmitrenko[1], Bert Rudels[2], Sergey A. Kirillov[1], Yevgeny O. Aksenov[3], Vidar S. Lien[4], Vladimir V. Ivanov[5,6], Ursula Schauer[7], Igor V. Polyakov[6], Andrew Coward[3], and David G. Barber[1]

[1]Centre for Earth Observation Science, University of Manitoba, Winnipeg, Manitoba, Canada, [2]Finnish Meteorological Institute, Helsinki, Finland, [3]National Oceanography Centre, Southampton, UK, [4]Institute of Marine Research, Bergen, Norway, [5]Arctic and Antarctic Research Institute, St. Petersburg, Russia, [6]Interanational Arctic Research Center, University of Alaska Fairbanks, Fairbanks, Alaska, USA, [7]Alfred Wegener Institute for Polar and Marine Research, Bremerhaven, Germany

Abstract The Atlantic Water flow from the Barents and Kara seas to the Arctic Ocean through the St. Anna Trough (SAT) is conditioned by interaction between Fram Strait branch water circulating in the SAT and Barents Sea branch water—both of Atlantic origin. Here we present data from an oceanographic mooring deployed on the eastern flank of the SAT from September 2009 to September 2010 as well as CTD (conductivity-temperature-depth) sections across the SAT. A distinct vertical density front over the SAT eastern slope deeper than ~50 m is attributed to the outflow of Barents Sea branch water to the Arctic Ocean. In turn, the Barents Sea branch water flow to the Arctic Ocean is conditioned by two water masses defined by relative low and high fractions of the Atlantic Water. They are also traceable in the Nansen Basin downstream of the SAT entrance. A persistent northward current was recorded in the subsurface layer along the SAT eastern slope with a mean velocity of 18 cm s^{-1} at 134–218 m and 23 cm s^{-1} at 376–468 m. Observations and modeling suggest that the SAT flow has a significant density-driven component. It is therefore expected to respond to changes in the cross-trough density gradient conditioned by interaction between the Fram Strait and Barents Sea branches. Further modeling efforts are necessary to investigate hydrodynamic instability and eddy generation caused by the interaction between the SAT flow and the Arctic Ocean Fram Strait branch water boundary current.

1. Introduction

The speculations of possible impacts of the North Atlantic circulation and the Gulf Stream on the conditions in the Arctic Ocean have a long history. They started before any reliable knowledge of the Arctic Ocean was available and focused on the possible effects that the advected oceanic heat could have on the ice cover in the Arctic Ocean. That sea ice was present and prevented the navigation had been proven by many futile attempts to sail the Northeast and the Northwest passages. However, it was suggested that the ice barrier was mainly confined to the continents where the river input reduced the salinity and the water would freeze. The warm and saline water from the Gulf Stream that was observed moving northward in the Norwegian Sea could continue into the Arctic Ocean and open a passage through the ice and also act to keep the central Arctic Ocean free of ice [*Petermann*, 1865; *van Campen*, 1876]. *Petermann* [1865] assumed that the most likely place for such a flow would be over the Barents Sea (henceforth Barents Sea Branch Water: BSBW, Figure 1a) and then into the Arctic Ocean east of Svalbard. When Nansen entered the Arctic Ocean on Fram he did not discover an ice-free Arctic Ocean, nor a passage kept free of ice by advected warm Atlantic Water. However, he found a subsurface layer of warm, saline water below a less saline and cold surface layer [*Nansen*, 1902]. Nansen considered that this warm layer derived from an inflow of Atlantic Water (Gulf Stream water) through Fram Strait (henceforth Fram Strait Branch Water: FSBW, Figure 1a) not the Barents Sea, although he earlier had accepted Petermann's view that the main inflow of Atlantic Water was likely to occur over the Barents Sea [*Nansen*, 1902].

This description has since pervaded and it has been the inflow of Atlantic Water and heat through Fram Strait that has drawn most attention. The old question has, however, not disappeared. It is still debated if the FSBW can have a significant effect on the ice cover in the Arctic Ocean and especially now, when the
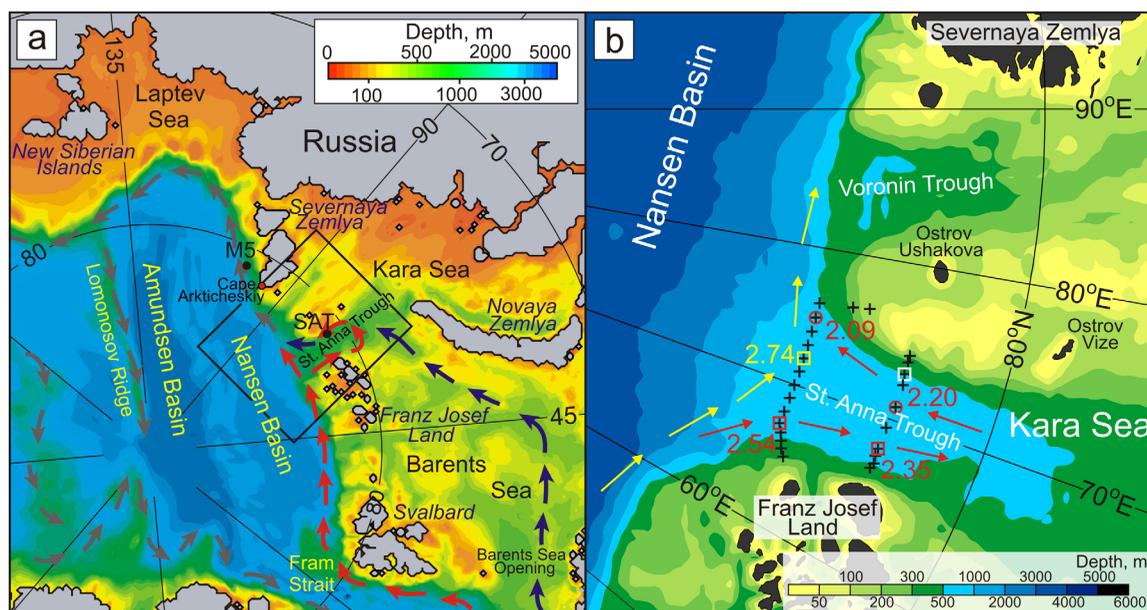
Figure 1. (a) A map of the Arctic Ocean. Arrows trace the Atlantic Water pathways; red and blue arrows show the Fram Strait and Barents Sea branches, respectively, of the Atlantic Water flow to the Arctic Ocean in accordance with *Rudels et al.* [1994]. Black circles mark the SAT and M5 moorings. The black rectangle encloses the northern Kara Sea with St. Anna Trough (SAT) and adjoining Arctic Ocean Nansen Basin enlarged in Figure 1b. (b) Arrows show the Fram Strait branch of the Atlantic Water inflow into the Arctic Ocean (FSBW) that recirculates in the SAT (red arrows) and follows the Nansen Basin continental margin (yellow arrows) following *Hanzlick and Aagaard* [1980] and *Rudels et al.* [1994]. Crosses show the positions of CTD stations taken in September 2009 at two sections crossing the SAT at ∼81°N and 82°N. Red squares and circles identify stations taken through the core of the SAT-circulating FSBW inflow and outflow to/from the SAT, respectively. The yellow square identifies station taken through the core of the FSBW boundary current, flowing along the Nansen Basin continental slope. The white square depicts SAT mooring position. Numbers show the FSBW core temperature (°C) in September 2009.

Arctic experiences a strong warming, heat from the Atlantic Water might add that crucial amount of heat needed to significantly reduce the ice cover. As the FSBW flows into the Arctic Ocean, its upper part becomes transformed by melting sea ice into a less saline upper layer that isolates the warm core from ice and atmosphere, although recent studies indicate that heat from the FSBW contribute to reduce the sea-ice cover along the FSBW pathway north of Svalbard, especially during winter [*Ivanov et al.*, 2012; *Onarheim et al.*, 2014]. In contrast, the BSBW inflow, although of similar magnitude as that through Fram Strait [*Blindheim*, 1989; *Ingvaldsen et al.*, 2004; *Beszczynzka-Möller et al.*, 2012], experiences strong transformations as it crosses the Barents Sea. In the southern part, cooling removes most of the heat of the Atlantic Water [e.g., *Årthun and Schrum*, 2010; *Smedsrud et al.*, 2013] and creates a cold and dense water mass [*Nansen*, 1906; *Midttun*, 1985; *Quadfasel et al.*, 1992]. In addition, ice formation and subsequent brine rejection over shallow banks creates cold and dense water that sinks to the bottom and fills the deepest part of the depressions [*Knipovitch*, 1905; *Nansen*, 1906; *Defant*, 1961; *Midttun*, 1985; *Martin and Cavalieri*, 1989; *Årthun et al.*, 2011]. In the northern part of the Barents Sea, the Atlantic Water interacts with sea ice to form a less saline upper layer, similar as north of Svalbard [e.g., *Rudels et al.*, 2004]. The density range of the BSBW thus increases and as it eventually enters the Arctic Ocean, mainly along the St. Anna Trough (SAT), but also along the Victoria Channel west of Franz Josef Land, it interacts with the Arctic Ocean water column over a large depth range [*Schauer et al.*, 1997; *Rudels and Friedrich*, 2000; *Rudels*, 2001; *Årthun et al.*, 2011]. The expected impact of the BSBW on the Arctic Ocean water column was an input of colder, less saline and dense water that entered the boundary current below the warm core of the FSBW [*Rudels et al.*, 1994; *Schauer et al.*, 1997]. Furthermore, the relatively cold and low-salinity BSBW was followed in the Amundsen Basin [*Schauer et al.*, 2002a] and into the Canada Basin [*McLaughlin et al.*, 2002].

More recently, it has been proposed that the BSBW also provides the relatively warm Atlantic Water observed in the Amundsen, Makarov, and Canada basins [*Rudels*, 2010, 2012; *Rudels et al.*, 2013]. This hypothesis was based on the fact that on the Kara Sea slope, just north of Severnaya Zemlya, two distinct cores of the boundary current could be identified. At the upper slope, around 400 m, a less saline and colder water column with maximum temperature of 1°C and a salinity of ∼34.85 was observed, while farther into the basin, above the 2000–3000 m isobaths, a warmer 3°C and more saline, 34.95, Atlantic core

was found. These two columns were identified as the BSBW on the upper part and the FSBW on the lower part of the slope.

Farther to the east, off the Laptev Sea slope, the two cores have merged and strong interleaving indicates isopycnal mixing between the cores and the maximum temperature and salinity are reduced to 2°C and 34.90. Beyond the Amundsen Basin and the Lomonosov Ridge, both the maximum temperature and salinity are lower than observed at the upper Kara Sea slope. Furthermore, the warm and saline FSBW appears confined to the Nansen Basin, indicating that the main part of the FSBW circulates within the Nansen Basin, while the BSBW supplies the Atlantic and intermediate waters in the other basins of the Arctic Ocean.

This interpretation was based on only a few observations in the SAT and on the continental slope between Franz Josef Land and Severnaya Zemlya. However, it is known that a fraction of warm FSBW, steered by the topography, enters the western SAT from the north and mixes with the colder BSBW before it recirculates back into the Nansen Basin along the SAT eastern slope (Figure 1a) [*Hanzlick and Aagaard*, 1980; *Schauer et al*., 2002b]. Hereinafter we refer to this fraction of the FSBW as SAT-circulating FSBW. Furthermore, mooring observations between Franz Josef Land and Novaya Zemlya indicate that very little of the water leaving the Barents Sea has temperatures close to 1°C as observed at the upper slope in the Kara Sea [*Loeng et al*., 1997; *Schauer et al*., 2002a; *Gammelsrød et al*., 2009]. It is then possible, and perhaps also plausible, that the warm core in the upper water column does not primarily derive from the BSBW, but mainly consists of FSBW that has been mixed into and joined the Barents Sea branch in the SAT. If this upper water column is the one that feeds the downstream basins beyond the Nansen Basin, the warmer water would to some degree be FSBW diluted by the BSBW. This possibility was recognized by *Rudels* [2012] and *Rudels et al*. [2013], but there judged less likely.

Based on observation from 1996, *Schauer et al*. [2002a] and *Rudels et al*. [2013] identified two dense water masses in the SAT. One cold ($T < -1°C$) and less saline water mass attached to the eastern slope and one denser, warmer ($T \approx -0.5°$) water mass in the deepest part of the trough. Both water masses were considered as BSBW modified by dense water created by brine rejection over the shallow areas in the Barents Sea. *Rudels et al*. [2013] suggested that the colder, less dense water might also be formed in the northern Kara Sea and sink directly into the trough. The denser, warmer water would mainly be Atlantic Water cooled and freshened by input of dense brine-enriched water formed mainly west of Novaya Zemlya, but possibly also over the Central Bank [*Schauer et al*., 2002a; *Årthun et al*., 2011]. Although being brine-enriched through ice formation, these water masses generally have lower salinities than the Atlantic Water flowing into the Barents Sea in the west [*Furevik*, 2001; *Årthun et al*., 2011]. In the 1980s the densest water over the Central Bank was observed when ice formation and brine rejection had taken place the previous winter. When warm, saline Atlantic Water was present over the bank, cooling did not appear to be sufficient to increase the density by the same amount and the water column was less dense [*Quadfasel et al*., 1992]. This is also obvious from the temperature-salinity (*TS*) diagram of observed bottom water on the Central Bank between 1970 and 2007 [*Årthun et al*., 2011, Figure 3]. However, recent observations indicate that the water over the Central Bank in 2007 was cold and saline Atlantic Water, denser than in the 1980s [*Rudels et al*., 2015]. Based on the 2008 data, *Lien and Trofimov* [2013] found that the Atlantic Water cooling with only insignificant dilution is sufficient to create a water mass with temperature exceeding 0°C, but still denser than the colder, less saline BSBW. This water mass was dense enough ($\sigma > 28.09$) to penetrate deep into the Arctic Ocean water column. This is in line with the finding by *Smedsrud et al*. [2013] of a positive correlation between heat inflow in the western Barents Sea and subsequent density of the outflow in the northeastern Barents Sea. *Lien and Trofimov* [2013] also identified the source of the less dense, colder water to the area around Franz Josef Land but they also noticed that the cooled Atlantic Water became colder and less saline as it passed into the Kara Sea and SAT. They therefore suggested another source of brine-enriched water just north of Novaya Zemlya that creates water dense enough to sink into and cool and fresh the Atlantic Water. *Lien and Trofimov* [2013] also suggested that the location of this source could vary with the atmospheric and sea ice conditions, and in the 1990s it might have been located farther south, at the banks west of Novaya Zemlya. The brine-enriched water would then interact with and cool the Atlantic water already in the eastern Barents Sea, creating the colder dense water observed in SAT in 1996 [*Schauer et al*., 2002a].

This study presents and analyzes recent observations from conductivity-temperature-depth (CTD) transects and mooring-based CTD and velocity measurements in the northern part of the SAT, with a focus on the interactions between the two Atlantic Water branches and how the characteristics of the water masses
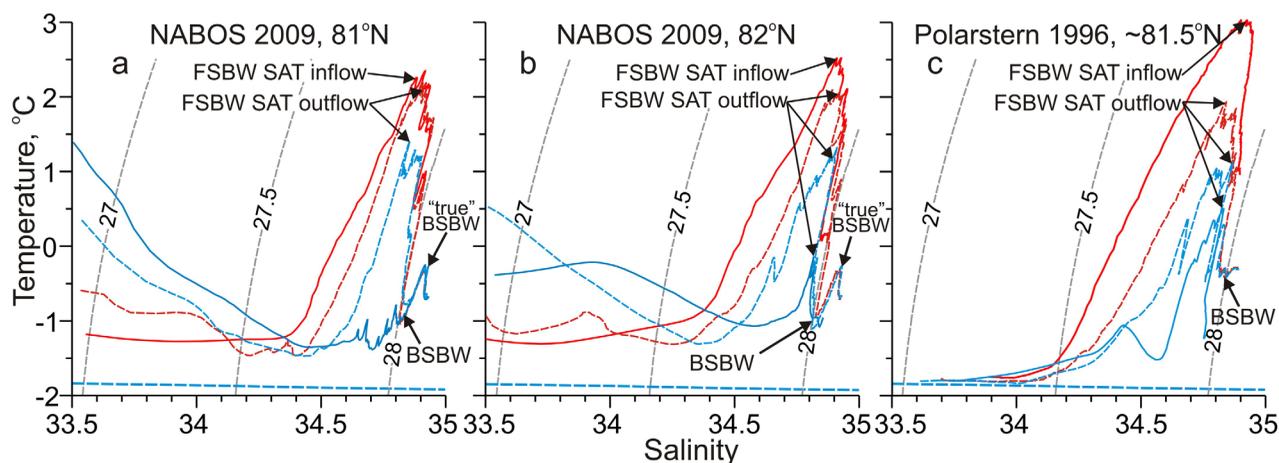
Figure 2. The *TS* diagrams for CTD profiles taken in the SAT (red—western slope, the FSBW SAT inflow: a = st. KD2309, b = st. KD8509, c = 81°27′N, 65°51′E; dashed red—low eastern slope, the FSBW SAT outflow: a = st. KD2509, b = st. KD7709, c = 81°17′N, 72°01′E; dashed blue—middle eastern slope, the FSBW SAT outflow: a = st. KD2609, b = st. KD7609, c = 81°23′N, 73°18′E; blue—upper eastern slope: a = st. KD2709, b = st. KD7509, c = 81°25′N, 74°24′E. Arrows mark the cores of the FSBW SAT inflow and outflow, BSBW and "true" mode of the BSBW. Gray-dashed lines are σ_0 isopycnals in kg m^{-3}.

relates to the variability of their upstream history and forcing. The downstream fate of the two branches is also followed as far as the Laptev Sea, where existing mooring and CTD observations will be related to this new and more detailed knowledge about the conditions in the SAT.

In August 2009, the international efforts by Russia (AARI), Germany (GEOMAR and AWI), and USA (IARC) resulted in the first-ever mooring deployment at the eastern slope of the SAT (Figure 1b). Our paper uses the 1 year (2009–2010) mooring records of temperature, salinity, and currents at fixed depth to resolve the two branches at the mooring site. Mooring observations were accompanied by the CTD profiles taken at transects crossing the SAT along 81°N (2008–2010) and 82°N (2009). We also invoke model simulations to assess mechanisms stipulating the Atlantic Water inflow to the Arctic Ocean.

The present paper follows up a recent study by *Dmitrenko et al.* [2014]. Using CTD profiles, velocity data, and model simulations, they examined vertical mixing and heat loss along the Atlantic Water pathway in the SAT and inferred an upward heat flux over the SAT eastern flank of O(30–100) W m^{-2}. This heat loss results in a consistently delayed freezeup during fall and a reduction in the sea-ice thickness during winter, as evident from sea-ice remote sensing. In contrast to *Dmitrenko et al.* [2014], here we focus on the lateral flow associated with the SAT outflow to the Arctic Ocean:

1. We examine the composition of the SAT outflow and, in particular, the fraction associated with BSBW. To this end, we revise the previous attribution of BSBW to the intermediate cooler and fresher water layer underlying the FSBW. We describe a warmer, saltier, and denser "true" mode of the BSBW (for more details see Figure 2), which constitutes a core of Atlantic origin within the BSBW. We also trace this "true" mode of the BSBW downstream of the SAT along the Laptev Sea continental margin.
2. We use the year-long mooring observations to assess the variability of the "true" BSBW at the SAT and in the Nansen Basin downstream of the SAT entrance.
3. We show compelling observational evidence of the strong outflow from the SAT along its eastern flank and discuss the role of thermohaline forcing of the SAT outflow using observational data and numerical ocean model simulations.

The paper is structured as follows: section 2 describes the observational data and model setup. Section 3.1 gives a census of the water masses in the region using the 2008–2010 temperature and salinity data from transects across the SAT. Section 3.2 focuses on temperature, salinity, potential density, and velocity data from the SAT mooring. Section 4.1 examines sources of the water masses which condition the Atlantic Water flow toward the Arctic Ocean through the SAT. Section 4.2 puts the findings into the context of the thermohaline structure of the boundary current downstream of the SAT with the aim of determining the possible sources of Arctic Intermediate waters. Section 4.3 analyses the year-long hydrographic time series

from the SAT mooring to investigate the driving mechanism of the SAT inflow into the Arctic Ocean, whereas section 4.4 examines the role of thermohaline forcing in conditioning the inflow. Finally, section 5 concludes the analysis and discusses its limitations.

2. Data and Methods

The data used in this study were collected from a conventional mooring with fixed-depth instruments deployed at 81°01.4′N, 73°02.5′E in the northern Kara Sea at the eastern slope of SAT (Figure 1a) in ~520 m water depth. This mooring collected data from 24 August 2009 to 22 September 2010. Initially the SAT mooring was designed to sample the cores of the SAT-circulating FSBW (~100–200 m) and the BSBW flowing into the Arctic Ocean through the SAT (~250–350 m). The SAT mooring was equipped with Sea-Bird Electronics, Inc. SBE-37s with CTD sensors placed at 140, 200, 260, 320, and 420 m, and Sea&Sun TD48M with temperature and turbidity sensors only placed at 510 m. The mooring also carried two Teledyne RD Instruments 300 kHz Workhorse Sentinel Acoustic Doppler Current Profilers (ADCPs) measuring velocity through the depth ranges 134–218 and 376–468 m.

The CTDs provided 30 min interval (TD48M) and 15 min interval (SBE-37s) records of conductivity, temperature, and pressure at fixed depths. Among all the salinity and/or temperature recorders, only probes at 140, 260, and 510 m provided the full 1 year data record. The 1 year of velocity data from the ADCPs were taken at 4 m depth intervals, with a 60 min ensemble time interval and 60 pings per ensemble.

For discussion, we also use data from the mooring M5 in the Nansen Basin north of Severnaya Zemlya (78°26′N, 125°37′E; Figure 1a), which collected data from 16 September 2006 to 17 September 2007. The mooring was equipped with a McLane Moored Profiler (MMP), an instrument that samples an underwater vertical profile along a mooring line at a speed of about 25 cm s^{-1}, with a sampling period of 0.5 s. The MMP was equipped with a CTD meter manufactured by Sea-Bird Electronics, Inc. (SBE), and an ACM (acoustic current meter), giving measurements of velocity (not used in this study). The profiler provided a 1 year long record between preprogrammed target depths of 156 and 2278 m.

Mooring-based observations were complemented by oceanographic CTD transects across the SAT (Figure 1b) taken from the icebreaker *Kapitan Dranitsyn* along ~ 81°N (24 October 2008) and along ~81°N and 82°N (22–23 August 2009 and 2–3 September 2009, respectively), and from the RV *Nikolay Evgenov* along ~81°N (22 September 2010). These sections were sampled using a shipboard SBE19+ CTD (2009–2010) and Lockheed Martin Sippican Expendable Bathythermographs – XBTs, and Expendable Conductivity, Temperature, and Depth Profilers – XCTDs (2008). Most of SBE19+ CTD casts were taken down to ~5 m above the seafloor. The CTD sensors were calibrated by the manufacturer (Sea-Bird Electronics, Inc.) before cruises. These data were complemented by oceanographic stations occupied across the SAT along ~81.5°N in August 1996 during the ARKXII cruise of the RV *Polarstern* [*Schauer et al.*, 2002b].

According to manufacturers' estimates, individual temperature and conductivity measurements are accurate to ±0.005°C and ±0.5 mS m^{-1}, respectively, for the SBE-19+, and to ±0.002°C and ±0.3 mS m^{-1}, respectively, for the SBE-37. XBT accuracy is ±0.05°C. XCTD accuracy is ±0.02°C, ±3 mS m^{-1}, and 2% of the depth range for temperature, conductivity, and depth, respectively. RDI ADCP precision and resolution are ±0.5% and ±0.1 cm s^{-1}, respectively. The ADCP velocity estimated error was of 0.5 cm s^{-1}. Compass accuracy is ±5°. At the M5 mooring, the MMP carried an SBE 41CP CTD sensor with temperature and conductivity measurement accuracies of ±0.002°C and ±0.0002 S m^{-1}, respectively.

In this study we use the ORCA025 Ocean General Circulation Model (OGCM) of the National Oceanography Centre Southampton, developed under the Nucleus for European Modeling of the Ocean (NEMO) framework for ocean climate research and operational oceanography (http://www.nemo-ocean.eu/). ORCA025 is extensively used in studying Arctic Ocean circulation [e.g., *Lique et al.*, 2009, 2010], freshwater exchanges with the Nordic Seas [*Jahn et al.*, 2012; *Marsh et al.*, 2010], sea ice [*Johnson et al.*, 2012], AW inflow into the Arctic [e.g., *Lique et al.*, 2009; *Popova et al.*, 2013], and Arctic ecosystem [*Popova et al.*, 2010, 2013]. The simulated Atlantic inflow though Fram Strait and Barents Sea is found to be in good agreement with observations [*Tsubouchi et al.*, 2012; *Popova et al.*, 2013].

ORCA025 is a z-level global coupled sea ice-ocean model, which includes the ocean circulation model OPA9 [*Madec and NEMO Team*, 2008] and the Louvain-la-Neuve sea ice model LIM2 [*Fichefet and Morales Maqueda*, 1997].

The ocean model is configured on a tri-polar Arakawa C-grid [*Arakawa*, 1966] with the model poles at the geographical South Pole, in Siberia, and in the Canadian Arctic Archipelago. The horizontal resolution is approximately 28 km at the equator, 6–14 km in the Arctic Ocean, and 12 km resolution in the area of interest, the Barents and Kara Seas including SAT. The model has 75 vertical levels with 19 levels in the upper 50 m and 25 levels in the upper 100 m. The thickness of top model layer is ∼1 m, increasing to 57 m at 600 m and to ∼204 m at 6000 m. Following *Barnier et al.* [2006], partial steps in the model bottom topography are implemented to improve model approximation of the steep seabed relief near the continental shelves, rendering the vertical model resolution in the SAT ∼50 m or finer.

For this study ORCA025 is forced by atmospheric 6 hourly fields 1958–2007 from the Common Ocean-Ice Reference Experiments (CORE2). The model forcing also includes climatological monthly continental runoff from *Dai and Trenberth* [2002]. The model is initialized from ocean temperature and salinity derived from a monthly climatology of the PHC2.1 database [*Steele et al.*, 2001]. The sea surface salinity is relaxed toward the monthly mean climatological values from WOA 2005 [*Levitus*, 1998a, 1998b] on the time scale of 180 days.

3. Results

3.1. CTD Transects

In the following, we build on the SAT circulation scheme suggested by *Hanzlick and Aagaard* [1980] (Figure 1b) that has been generally confirmed based on the 1996 cross-trough section reported in [*Schauer et al.*, 2002a]. The CTD, XBT, and XCTD sections taken across the SAT in 2008–2010 show the basic oceanographic patterns of the waters flowing in and out of the Nansen Basin through the SAT (Figures 3 and 4). The cross section along 82°N taken in 2009 is dominated by a saline, warm water mass that extends from the western flank almost to the opposite side of the trough (Figure 3). We identify this water as the core of the FSBW flowing toward the northern Kara Sea along the SAT western flank. It is traced by the intermediate (100–120 m) temperature maximum of 2.54°C at 82°N (Figures 1b and 2b) and 2.35°C further downstream at 81°N (Figures 1b and 2a). Two warm cores are identified on both the 81°N and the 82°N sections (Figures 3 and 4). The FSBW at the eastern part of the trough shows lower core temperatures decreasing from 2.2°C at 81°N (station KD8509; Figures 1b and 2a) to 2.09°C over the SAT mouth at 82°N (KD2309; Figures 1b and 2b). Moreover, the CTD profile taken in 2009 in the central part of the SAT mouth at 82°N (station KD8009; Figures 1b and 3a) shows an intermediate temperature maximum of 2.74°C that exceeds those for the FSBW inflow into the SAT by 0.2–0.4°C. One possible explanation is that this maximum is due to the boundary current meandering in the trough and bringing warmer FSBW (Figures 1 and 3a; for more details see *Dmitrenko et al.* [2014]). A strong temperature and salinity front is present in the eastern part of the trough and the temperature and salinity maxima observed over the deeper part of the eastern flank are much cooler and less saline than farther to the west. Below the temperature and salinity maxima a cold, low-salinity water mass is present, which extends to and cover the upper part of the eastern flank (Figure 4). At ∼81°N, the bottom layer on the deepest part of the flank and in the central part of SAT is again warmer, −0.5°C and more saline ∼34.9 (Figure 4). This structure is in general agreement with measurements taken in 1996 (Figure 2c). The interpretation of this structure is that most part of the trough is dominated by the entering and recirculation of the FSBW, but in the eastern part an outflow of colder and denser water from the Barents Sea takes place.

The CTD, XBT, and XCTD sections taken across the SAT along 81°N in 2008–2010 consistently show at least three water masses occupying the SAT eastern flank below the halocline layer. The FSBW, which outflows the SAT northward, is traced by the intermediate warm (>0°C) and saline water mass in 50–450 m (Figure 4). The extent of this water on the CTD transects varies from year to year. For example, in 2010 the FSBW was displaced westward, away from the SAT eastern flank by a cooler (∼−1°C) and fresher water mass (Figures 4c and 4f). This less saline water occupies the whole water column beneath the summer mixed layer above the upper eastern flank of SAT (∼74°E) and descends obliquely almost to the bottom in the middle of the SAT (∼71°E) (Figure 4). *Schauer et al.* [2002a] linked this water to the BSBW modified during transition across the Barents Sea through atmospheric cooling and lateral mixing with the Scandinavian river runoff present in the Norwegian Coastal Current and the Murman Coastal Current. *Rudels et al.* [2013] suggested that this water also
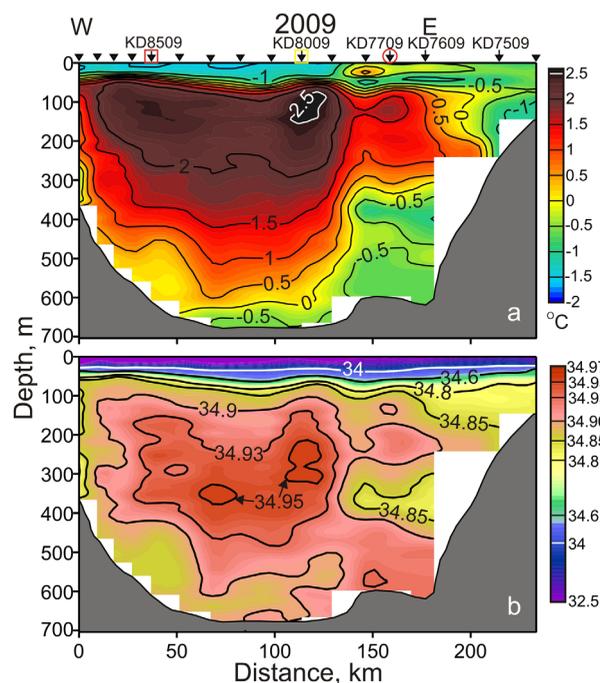
Figure 3. 10 m binned cross-trough sections of (a) temperature (°C) and (b) salinity taken in September 2009 along ~82°N. Blank areas represent missing data. Triangles on the top identify positions of CTD stations. Following Figure 1b, red square and circle identify stations taken through the core of the FSBW inflow and outflow to/from the SAT, respectively, with their reference numbers on the top. Yellow square identifies station taken through the core of the FSBW boundary current.

might be modified and/or formed over the shallow Kara Sea shelf just east of the SAT and then sink down the eastern flank into the trough.

The Barents Sea outflow also comprises the denser, saltier and warmer water mass that occupied the bottom layer over the middle and low SAT eastern flank in 2008 and 2010 (Figures 4a, 4c, 4d, and 4f). This water exhibits a substantial interannual variability. In 2008, it was substantially warmer (by about 0.5–0.7°C) compared with the overlying water layer, but still significantly cooler than the FSBW at the SAT eastern flank (Figures 4a–4c). The situation in 2010 was qualitatively consistent with that in 2008, but the temperature of the bottom layer was much lower, varying from −1 to −0.4°C. In 2009, however, the warmer bottom water was not clearly traceable along 81°N. This is consistent with the CTD transect taken in 1996 across the SAT at ~81°N that shows no warmer water near the seafloor [*Schauer et al.*, 2002a; see also *Rudels et al.*, 2015, Figure 2]. As for the 2009 cross-trough section along 81°N, the 2009 transect along 82°N shows similar patterns with no warm bottom layer over the eastern flank of the SAT

(Figure 3a). The warmer and saltier bottom layer consisted of a relatively higher fraction of warm and saline Atlantic Water compared with the overlying BSBW water. Thus, we consider this warmer and saltier bottom water to be a "true" mode of the BSBW.

In the following we formally assign the "true" mode of the BSBW in the SAT to the salinity $S > 34.9$ and temperature $T > 0°C$. The layer of the "true" BSBW is centered at potential density $\sigma_0 \sim 28.04$ kg m^{-3}. The BSBW with a lower fraction of the Atlantic Water at $T < 0°C$, $S > 34.75$ centered at $\sigma_0 \sim 28$ kg m^{-3} resides between the "true" BSBW and FSBW. The FSBW in the SAT outflow at $T > 0°C$ and $34.75 < S < 34.95$ contains the highest fraction of Atlantic Water. It is centered at $\sigma_0 \sim 27.85$ kg m^{-3} overlying the BSBW (Figure 2). This classification follows that used by *Lien and Trofimov* [2013] for describing the Barents Sea outflow to the northern Kara Sea. For the Barents Sea, the BSBW in the SAT by $T < 0°C$ and $S > 34.75$ was referred to as Cold Deep Water [*Gammelsrød et al.*, 2009; *Årthun et al.*, 2011; *Lien and Trofimov*, 2013]. We also argue that the definition of the BSBW in the SAT is somewhat arbitrary, and the BSBW at $28.0 < \sigma_0 < 28.02$ kg m^{-3} and $T \leq 0°C$ seems to be already constituted by some fraction of the "true" BSBW (Figure 2).
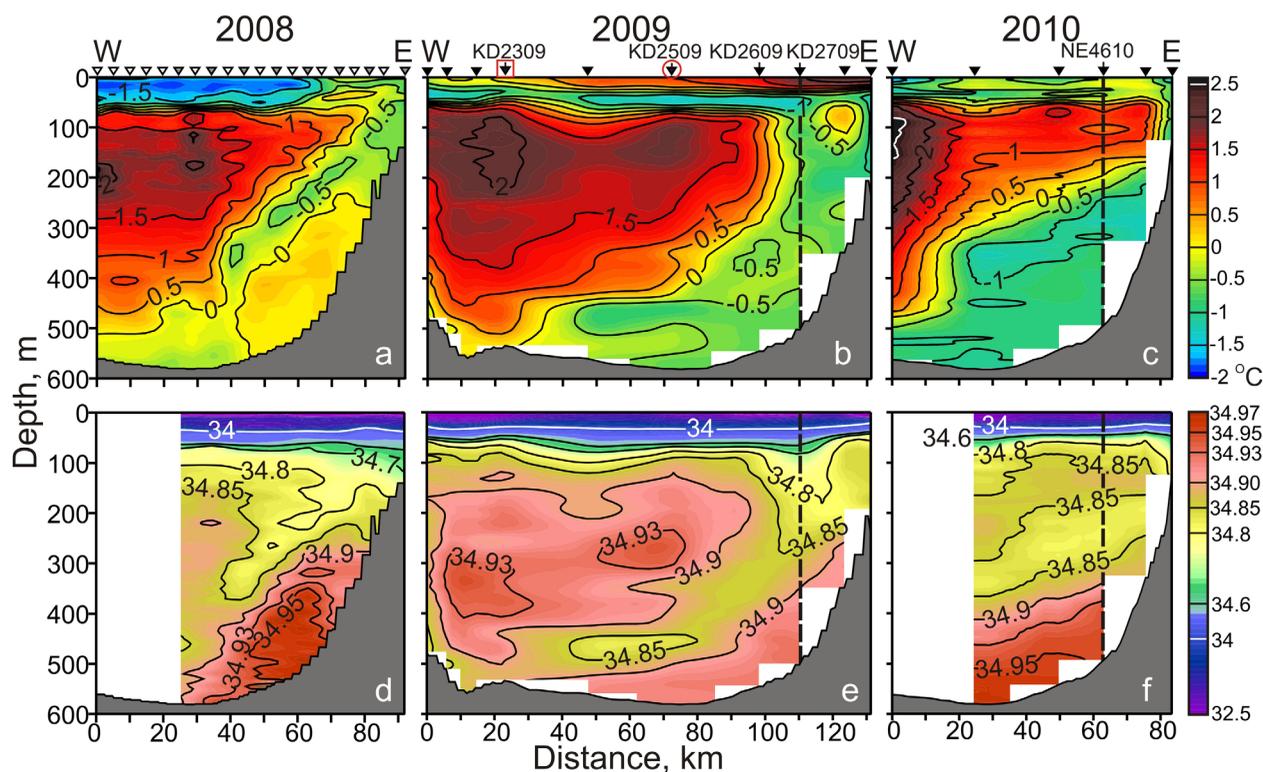
The cross-trough distribution of the potential density in 1996 and 2008–2010 consistently shows the denser water occupying the eastern flank of the SAT below the halocline layer (>50 m) in 2008–2010 (Figures 5a–5c) and extending to the upper layer in 1996 [*Schauer et al.*, 2002a, Figure 2]. At 150 m, the density gradient across the SAT eastern flank along 81°N varies from 0.09×10^{-2} kg m^{-3} km^{-1} in 2010 (Figure 5c) to 0.18×10^{-2} kg m^{-3} km^{-1} in 2008–2009 (Figures 5a and 5b). At 300 m, the cross-slope density gradient in 2008–2010 shows more uniform values of $\sim 0.16–0.18 \times 10^{-2}$ kg m^{-3} km^{-1} (Figures 5a–5c). For comparison, in 1996 the density gradient across the SAT eastern flank was $\sim 0.22 \times 10^{-2}$ and 0.09×10^{-2} kg m^{-3} km^{-1} at 150 and 300 m, respectively [*Schauer et al.*, 2002a].

3.2. Mooring Observations
The SAT mooring provides temperature and salinity records that resolve the water column beneath the halocline layer from 140 m depth to 420 m depth for salinity and to 10 m above the seafloor for temperature (Figure 6).

Figure 4. 10 m binned cross-trough sections of (a–c) temperature (°C) and (d–f) salinity taken along ∼81°N in (left) October 2008, (center) September 2009, and (right) September 2010. Blank areas represent missing data. Vertical-dashed line shows mooring position. Black, gray, and white triangles on the top identify positions of CTD, XCTD, and XBT stations, respectively. Following Figure 1b, red square and circle identify stations taken through the core of the FSBW inflow and outflow to/from the SAT, respectively, with their reference numbers on the top.

The records from 140 and 200 m associated with the FSBW are relatively well correlated (correlation is 0.68 for temperature and 0.60 for salinity) that in general confirms a similar origin for the water layer in 140–200 m. Only December 2009 shows an exception with salinity and temperature maximum at 200 m lagging those at 140 m by ∼2 weeks (Figures 6a and 6b). Except December 2009–February 2010, temperatures and salinities at 140 m exceed those at 200 m by 0.62 ± 0.21°C and 0.016 ± 0.011, respectively (Figures 6a and 6b). This is consistent with temperature and salinity sections taken across the eastern flank of the SAT that show cooling and freshening with depth beneath the FSBW core (Figures 3 and 4) down to ∼250–300 m.

For 260–510 m, temperature shows rather uniform values with the temperature scatter for different depths within ± 0.25°C. The only notable exception occurs in February–April 2010 (period III in Figure 6a) when the temperature of the bottom layer (510 m) exceeds that for 260–320 m by ∼0.6°C. We also note that in 10 January to 18 February 2010 the lower layer (420–510 m) temperature was the highest in the entire water column covered with temperature observations, showing a mean temperature of ∼0.1°C (Figure 6a). In fact, in 10 February 2010 the bottom layer temperature at 510 m exceeds the temperature in the FSBW by ∼0.7°C. The preceding event in 7–15 January shows almost uniform temperatures in 140–420 m of about -0.1 ± 0.2°C indicated by dashed square in Figure 6a. This event is associated with significant cooling (by ∼1°C) of the intermediate water layer and warming (by ∼0.5°C) of the underlying water. Moreover, the entire period II in Figure 6a shows an exceptionally small temperature difference throughout the water column resolved with data, with the standard deviation from the mean ± 0.26°C. For example, for the following period III the standard deviation of the mean (± 0.74°C) is about 3 times higher (Figure 6a).

In contrast to the quasi-uniform temperatures, salinities in 260–420 m exhibit a tendency to increase with depth (Figure 6b). Except the low-salinity event in the FSBW layer (140–200 m) in December 2009 to February 2010, among all depths covered with CTD data the salinity at 260 m is the lowest (compare 34.82 ± 02 at 260 m with 34.85 ± 02 at 140 m, 34.83 ± 02 at 200 m, and 34.88 ± 03 at 320 m). Maximum salinity of
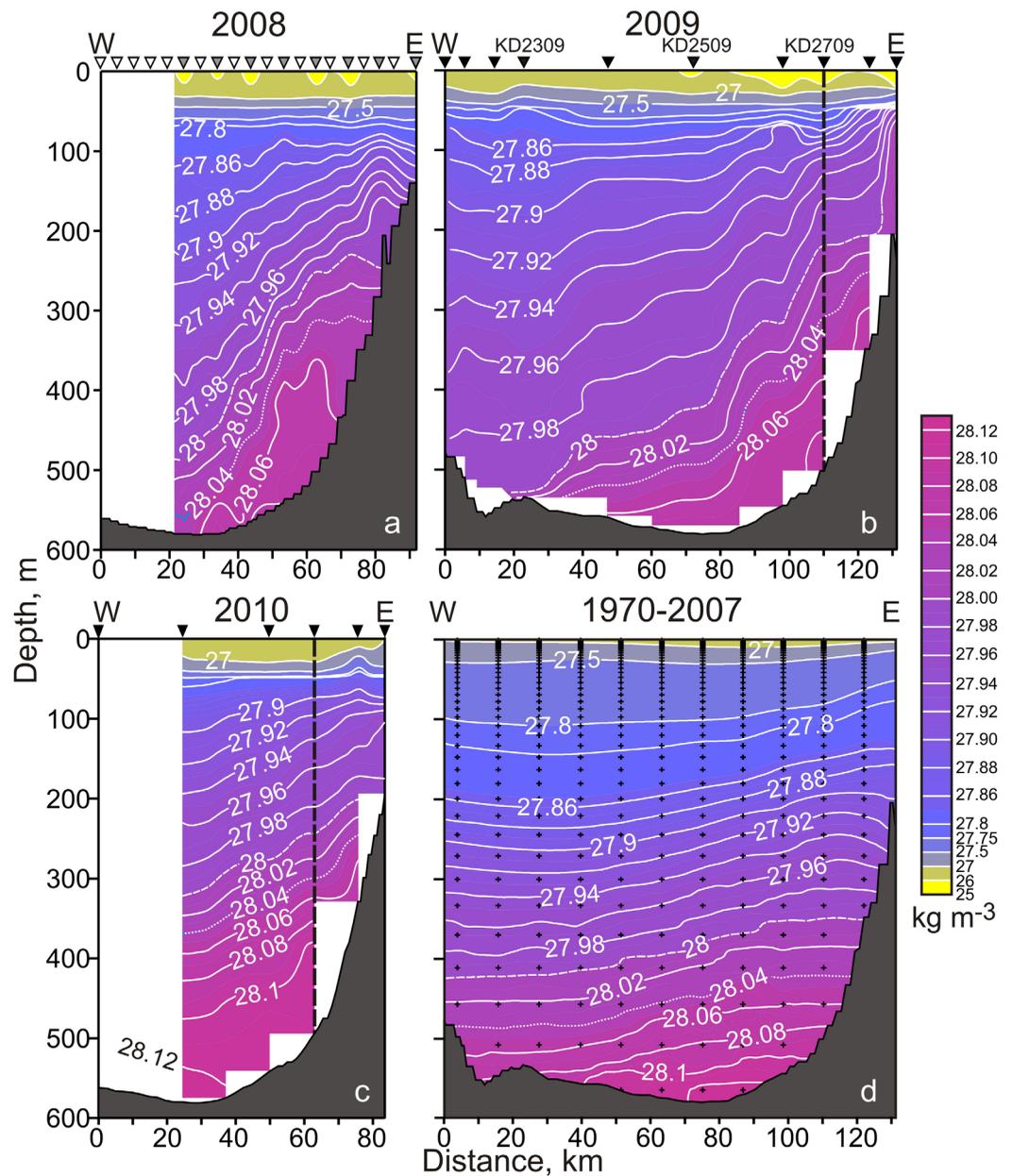
Figure 5. 10 m binned cross-trough sections of potential density (σ_0, kg m^{-3}) along 81°N for (a) October 2008, (b) September 2009, (c) September 2010 after *Dmitrenko et al.* [2014], and (d) long-term (1970–2007) mean compiled using annual-mean model simulation data. White dashed and dotted lines highlight σ_0 contours 28 and 28.04 kg m^{-3}, respectively. (d) Crosses depict levels used in simulations. Other designations are similar to those in Figure 4.

~34.97 is observed at 420 m in December 2009 to January 2010, the period when the salinity at 140 m shows a minimum of ~34.77 that corresponds to the maximum vertical salinity gradient for the entire period of mooring observations. Moreover, period II with exceptionally strong vertical salinity stratification is associated with an extremely low-temperature difference in 140–510 m (Figures 6a and 6b).

In contrast to temperature and salinity, the potential density time series are well correlated in 140–320 m. The only notable exception is in December 2009 to April 2010 that shows a negative density trend at 320 m in contrast to a positive trend in 140–260 m (Figure 6c). While the general tendency of the density time series at 320 and 140–260 m is different, for the synoptical time scale (~5–12 days) the density changes down to 320 m are highly coherent (Figure 6c).
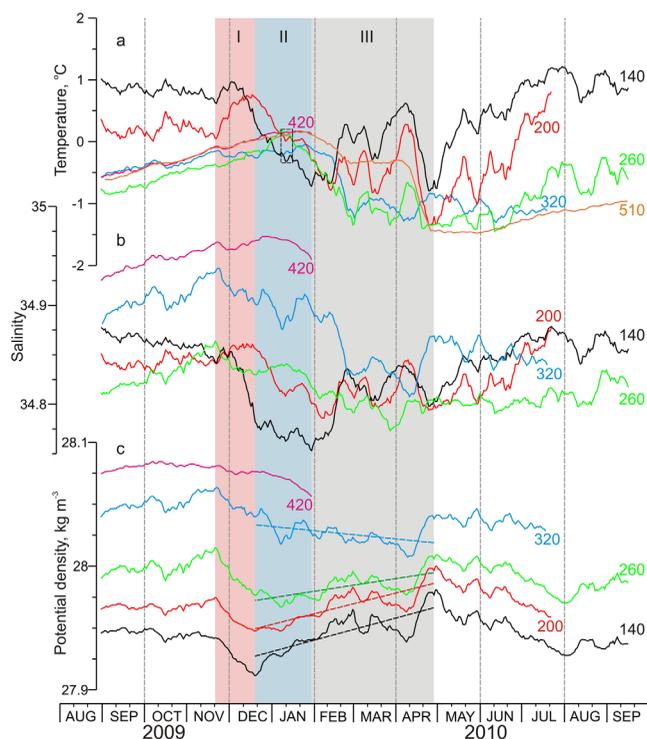
Figure 6. 14 day running mean of (a) temperature ($^\circ$C), (b) salinity, and (c) potential density (σ_0, kg m^{-3}) from the SAT mooring: black = 140 m, red = 200 m, green = 260 m, blue = 320 m, violet = 420 m, and orange = 510 m. Red, blue, and gray-shading highlight periods with different tendency of temperature, salinity, and σ_0 (see text for more explanations). Dashed lines show the linear trends of σ_0.

The temperature record from 510 m depth is also consistent with the presence of "true" BSBW. For example, in January 2010 the water temperature in 510 m shows ~0.2°C—the maximum temperature through the entire water column resolved with CTD data. This temperature is 0.5°C higher than at 140 m (Figure 6a). Moreover, the temperature at 420 m closely resembles that for 510 m, suggesting that at least the 100 m thick bottom layer with $\sigma_0 > 28.05$ kg m^{-3} is comprised by "true" BSBW of advective origin. However, later in the year the temperature at 510 m drops below -1°C, indicating that the "true" BSBW only occasionally supplies water to the Arctic Ocean, and also suggesting that cold, brine-enriched water could comprise the densest part of the SAT outflow from the Barents Sea. However, because no salinity observations are available from 510 m this cannot be confirmed (Figure 6a).

The velocity records show relatively stable, nearly barotropic northward flow aligned to ~2° in 140–220 m and to ~11° in 380–460 m that is consistent with the orientation of the SAT eastern flank (Figures 1 and 7). The flow speed increases slightly with depth from 17 $\pm$ 7 cm s^{-1} at 140 m to 20 $\pm$ 7 cm s^{-1} at 220 m (Figure 7a), 21 $\pm$ 5 cm s^{-1} at 380 m, and 23 $\pm$ 5 cm s^{-1} at 460 m (Figure 7b). Velocity time series from the different depths are entirely coherent, with a maximum northward flow of 40 cm s^{-1} synchronously observed at all levels in 18 January 2010 (Figure 8). The only event of southward flow (7 cm s^{-1}) was observed in 20 February 2010. In November 2009 to April 2010 (periods I–III, Figure 8), the velocity record is dominated by about 50 day periodicity with velocity amplitude of ~7 cm s^{-1}. In December 2009 to April 2010 (periods II–III, Figure 8), this periodicity is superimposed onto a negative trend in the meridional velocity component with the velocity magnitude decreasing from 22–25 to 12–15 cm s^{-1} (Figure 8). We note that this slowing of the SAT outflow is associated with a positive trend in potential density in the 140–260 m depth range.

4. Discussion

Several questions are addressed in this section. First, we elaborate on the sources of the water masses observed in the SAT outflow putting our findings in context of preceding research in this area (section 4.1). Second, we trace the SAT water masses at mooring M5 deployed downstream of the SAT on the continental slope of Severnaya Zemlya Archipelago in 2006–2007 (Figure 1a; section 4.2). Then, we focus on explaining
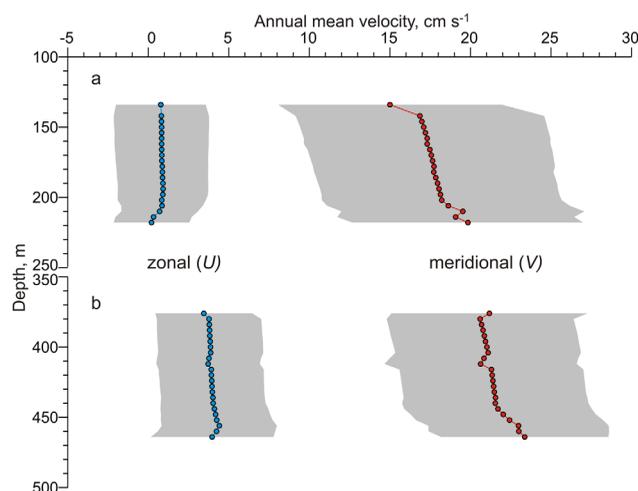
Figure 7. Year-mean vertical profiles of cross-trough (*U*, blue) and along-trough (*V*, red) velocity (cm s^{-1}) derived from yearlong ADCP records from the (a) upper and (b) low ADCPs. Gray shading shows ±one standard deviation of the mean.

the variability in temperature, salinity and density at the SAT mooring (section 4.3). Finally, we discuss the role of thermohaline forcing of the SAT outflow using numerical simulations of cross-trough density distribution and water dynamics over the SAT eastern flank (section 4.4).

4.1. Thermohaline Structure of the Atlantic Water Flow to the Arctic Ocean Through the SAT: Local Modifications

The SAT flow into the Nansen Basin is conditioned by interaction between the SAT-circulating FSBW and the BSBW, which enters the Barents Sea through the Barents Sea opening (Figure 1a). In the Barents Sea, warm (5–6°C) and saline (35.05–35.15) BSBW [*Furevik*, 2001] experiences transformation to cooler and fresher water through direct atmospheric cooling [e.g., *Aksenov et al.*, 2010; *Årthun and Schrum*, 2010; *Smedsrud et al.*, 2010, 2013], and through net precipitation and freshwater input from the less saline coastal current and to a lesser extent by direct river runoff [e.g., *Steele et al.*, 1995]. Furthermore, the BSBW is affected by sea-ice formation over the shallow banks and coastal polynyas [*Martin and Cavalieri*, 1989; *Årthun et al.*, 2011]. This creates brine-enriched dense water that sinks into and transform the denser part of the BSBW. The BSBW modification is also forced by changes in annual net ice import from the Arctic Ocean to the Barents Sea [*Aagaard and Woodgate*, 2001; *Ellingsen et al.*, 2009]. The strongly modified BSBW eventually flows into the Nansen Basin through the SAT with temperatures below 0°C and salinities between 34.7 and 34.9 [*Schauer et al.*, 2002a].

4.1.1. Subsurface Layer

Over the SAT eastern flank, the upper BSBW exhibits temperatures below 0°C, salinity in the range 34.7–34.85 and a corresponding σ_0 below 27.86 kg m^{-3}. The relatively low salinity indicates a substantial fraction of coastal water. Here this part of the BSBW partly merges with a fraction of the warm, intermediate FSBW ($T \sim 2.5$°C) entering the SAT from the north and steered by the topography [*Hanzlick and Aagaard*, 1980; *Schauer et al.*, 2002a; *Aksenov et al.*, 2010, 2011]. The CTD profiles taken in 2009 through the FSBW at the eastern SAT flank at 81°N and 82°N indicate significant cooling and freshening in the upper layer of the FSBW compared with the FSBW entering the SAT (Figures 2a, 2b, 3a, and 4b). This is also in agreement with the CTD profiles taken in 1996, 2008, and 2010. The freshened, cooled core that leaves the SAT, however, becomes denser than the entering FSBW core. This suggests that the main transformation of the FSBW is due to almost isopycnal mixing between BSBW and FSBW. Here we may add that it was the much lower temperature maximum over the eastern flank of the SAT and also over the upper part of the Kara Sea slope. This led *Rudels et al.* [2013] to assume that the temperature maximum over the SAT eastern slope constituted a part of the BSBW. In a sense it does, but the temperature and the salinity have increased by mixing with FSBW, which might comprise 50% of the resulting water mass.

In the SAT, the warm core of the SAT-circulating FSBW may also interact with sea ice [*Dmitrenko et al.*, 2014], which reduces the ice cover and transforms the upper part of the water column into a less saline
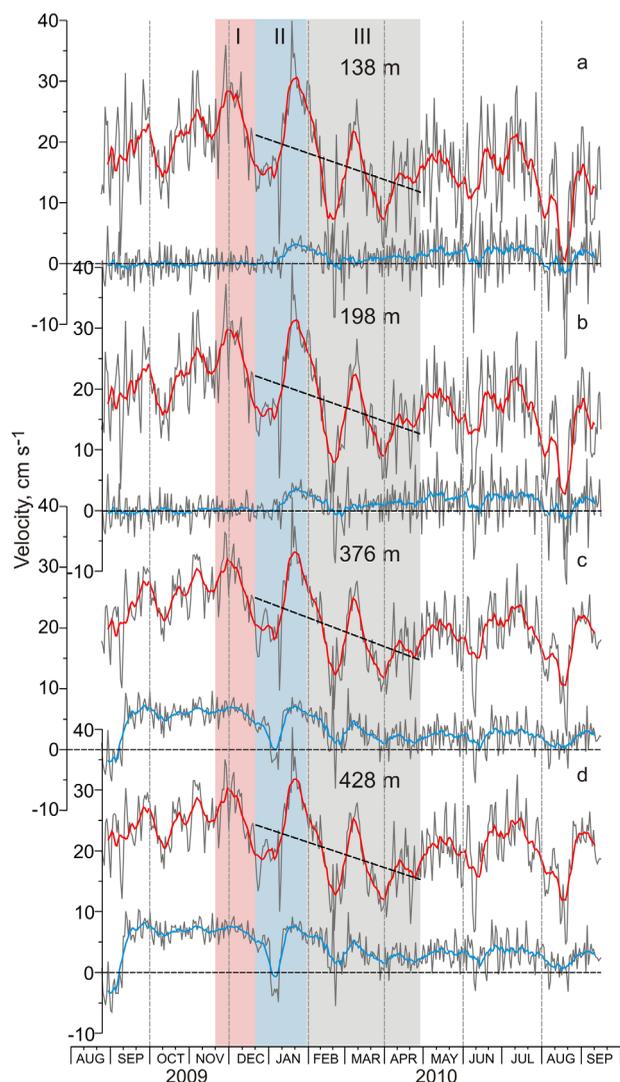
Figure 8. The year-long daily mean time series of velocity (cm s^{-1}) from (a) 138 m, (b) 198 m, (c) 376 m, and (d) 428 m. The 14 day running mean of along-trough and cross-trough velocity shown by red and blue lines, respectively. Other designations are similar to those in Figure 6.

surface layer by mixing with sea ice meltwater. Together with the upper layer formed north of Svalbard and in the northern Barents Sea, this water eventually supplies the lower halocline in the Arctic Ocean.

4.1.2. Intermediate and Bottom Layer

In 1996, the water at the SAT eastern flank was cold ($\sim -1°C$), but in the central SAT this cold water was overlying a slightly warmer (up to $-0.5°C$) and saltier bottom layer with salinity between 34.8 and 34.9. Based on this record, *Schauer et al.* [2002b] suggested that the warmer and saltier bottom layer is most likely not cooled Atlantic Water from the Barents Sea branch since its salinity is too low. The lower salinity and temperatures were explained by mixing with colder, brine enriched but less saline water, possibly formed over the shallow shelf west of Novaya Zemlya. In contrast, at cross-SAT section taken in 2008, warmer and saltier bottom layer occupied the SAT eastern flank (Figure 4). Moreover, in 2008 the maximum temperature at the bottom layer (0.2°C) was associated with salinity around 34.97 (Figures 4a and 4d). The mooring record from 420 m also shows similar maxima (Figure 9a). This temperature maximum is significantly lower than that of Atlantic Water in the western Barents Sea, but the relatively high salinity implies lower contribution of transformed water from shallow areas and/

or by net precipitation and river runoff water. Hence, this is "true" mode of the BSBW, which constitutes a core of Atlantic origin within the BSBW.
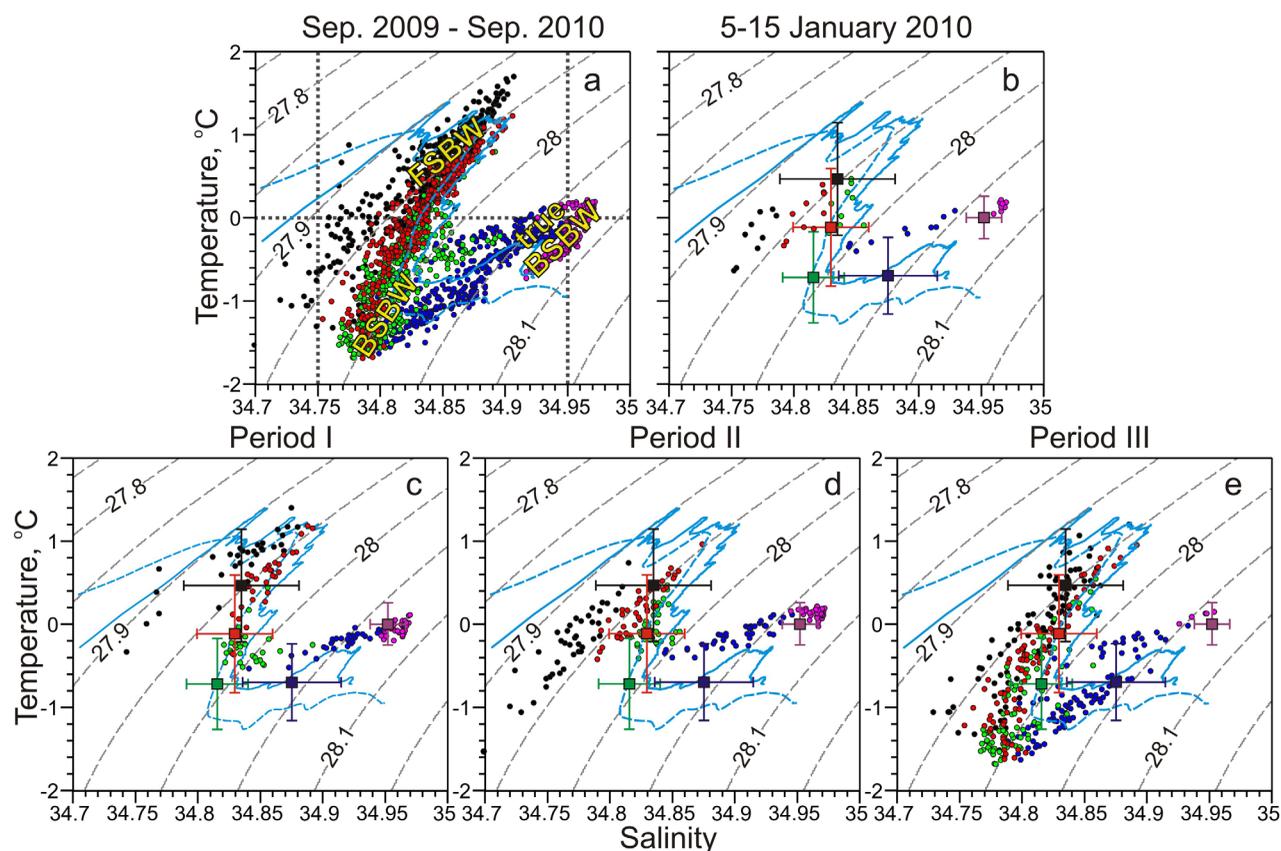
Lien and Trofimov [2013] observed and traced this water mass in August–September 2008 on several sections between Novaya Zemlya and Franz Josef Land as well as across the SAT at $\sim 81°N$. So, the near-bottom layer of saltier and warmer water at the eastern slope in the SAT can be interpreted as a continuation of the warmer and saltier bottom layer found upstream northward off Novaya Zemlya. Relatively high bottom layer salinity in 2008—2010 (Figures 4d–4f) also results in higher $\sigma_0 > 28.04$ kg m^{-3} (Figures 5a–5c) exceeding that reported in *Schauer et al.* [2002a] by >0.05 kg m^{-3}. In December 2009, at 420 m the σ_0 of the salinity/temperature maximum was recorded as high as 28.07 kg m^{-3} (Figures 6 and 9a).

The observations in 2008, 2009, and 2010 showed that the characteristics of the densest contribution from the SAT outflow vary considerably in time. While the observations in 1996 revealed a bottom temperature of about $-0.5°C$, the temperature in 2008 was above 0°C and the salinity was higher than that in 1996 [*Schauer et al.*, 2002a]. This strongly suggests that the water mass transformations taking place in the Barents Sea vary significantly. The appearance of the "true" BSBW can be associated with increasing temperature and salinity of the BSBW in the Barents Sea opening [e.g., *Skagseth et al.*, 2008; *Lien and Trofimov*, 2013] and consequently

Figure 9. The *TS* scatterplot of the daily mean temperature and salinity time series from the SAT mooring. Blue solid and dashed lines show the CTD casts taken nearby SAT mooring in September 2009 (st. KD2609) and September 2010 (st. NE4610), respectively. Black, red, green, blue, and violet circles show data from SBE-37s placed at 140, 200, 260, 320, and 420 m, respectively. *TS* scatterplots are shown for (a) yearlong record, (b) 5–15 January 2010, (c) period I: 20 November–20 December 2009, (d) period II: 20 December 2009–30 January 2010, and (e) period III: 30 January–28 April 2010 highlighted in Figures 6 and 8 with pink, blue, and gray shading, respectively. (a) Black-dotted lines indicate the bounds defining the different water masses over the SAT eastern slope: the FSBW, BSBW, and "true" mode of the BSBW (see text for more explanations). Note that the definition of the BSBW is arbitrary, and the BSBW at $28.0 < \sigma_0 < 28.02$ kg m^{-3} and T ≤ 0°C is already constituted by some fraction of the "true" BSBW. (b–e) Error-bared square show year mean ± standard deviation. Gray-dashed lines are σ_0 isopycnals in kg m^{-3}.

less sea ice within the Barents Sea [*Årthun et al.*, 2012]. The AW warming of the 1990s captured by SAT observations in 1996 was associated with the BSBW temperature and salinity in the Barents Sea opening of 5.5°C and 35.07 [*Furevik*, 2001]. In 2007, they were recorded at their maximum of 6.2°C and 35.15 (R. Ingvaldsen, personal communication, 2014). The relatively high salinity of the "true" mode of the BSBW suggests that the transformation of the BSBW occurs mainly through direct atmospheric cooling with insignificant freshwater input during periods of reduced sea-ice cover in the Barents Sea. *Aagaard and Woodgate* [2001] suggested that the freshening of the Atlantic Water passing over the Barents Sea was at least partly (35%) due to the melting of sea ice and the entrainment of meltwater into the Atlantic Water. A reduction or removal of this meltwater input could result in a mode of BSBW with temperature/salinity of ∼0°C/34.95 and σ_0 exceeding that for the BSBW by 0.06 kg m^{-3} [*Aagaard and Woodgate*, 2001]. These estimates are quantitatively consistent with our observations, definition of the "true" mode of the BSBW and model simulations by *Årthun et al.* [2011]. *Årthun et al.* [2011] further show that during warm periods with high Atlantic Water inflow to the Barents Sea, the cold and dense water formation on the Barents Sea banks and export to the Arctic Ocean is strongly reduced, but the export of water masses with $T > 0$°C is increased. Moreover, based on model simulations, *Smedsrud et al.* [2013] found a positive correlation between the heat transport into the Barents Sea in the west and the density of the BSBW leaving the Barents Sea to the east.

For the merged Atlantic Water branches downstream of the SAT mouth, the intrusion of cooler and fresher BSBW maintains the knee on the *T-S* plane at $\sigma_0 = 28.00 \pm 0.02$ kg m^{-3} [e.g., *Rudels et al.*, 2000; *Woodgate et al.*, 2001; *Dmitrenko et al.*, 2008, 2009a] that remains recognizable over the Siberian shelf junction with Lomonosov Ridge [*Woodgate et al.*, 2001; *Dmitrenko et al.*, 2009b] and even in the Canada Basin [*McLaughlin*

et al., 2002]. This structure was also noticed in the SAT by *Schauer et al.* [2002a, 2002b]. Complementing the paper by *Schauer et al.* [2002a], our CTD data and mooring records clearly show that this knee is maintained in the *TS* plane of the SAT outflow by the (i) warm ($>>0°C$) and saline FSBW ($\sigma_0 \sim 27.92 \pm 0.01$ kg m^{-3}), (ii) cooler ($<0°C$) and fresher BSBW ($\sigma_0 \sim 28.00 \pm 0.02$ kg m^{-3}), and (iii) warmer ($\sim 0°C$) and saltier "true" mode of the BSBW ($\sigma_0 \sim 28.04$ kg m^{-3}; Figures 2–4 and 9). Our results clearly indicate that the denser "true" BSBW, flowing toward the Arctic Ocean through the SAT below the BSBW, constitutes the water mass underlying the knee in the *TS* plane. In the winter 2009–2010, the bottom water in the SAT was colder than the preceding and the following winter, and it formed a temperature and salinity minimum at the bottom. This indicates that freezing and brine rejection had created dense bottom water that had not been mixed into the overlying cooled Atlantic Water, but was still identified in the deepest part of the SAT. Hence, the presence of the "true" mode of the BSBW is subject to variability both within and between years. In the following section, we focus on the temperature and salinity records from the M5 mooring located downstream the SAT mouth (Figure 1a) to asses characteristic patterns of temperature and salinity within the $\sigma_0 = 28.00$–28.06 kg m^{-3}—the σ_0 range that corresponds to the BSBW and its "true" mode in the SAT (Figures 2a, 2b, 4, and 5).

4.2. Thermohaline Structure of the Atlantic Water Flow to the Arctic Ocean Through the SAT: Far-Field Effects

The year-long record of temperature and salinity at mooring M5 shows that the $\sigma_0 = 28.00$ kg m^{-3} (this σ_0 contour roughly tracing the core of the BSBW (Figures 2, 4, and 5)) matches the depth ~ 800 m. The range $\sigma_0 = 28.00$–28.06 kg m^{-3} matches 800–1800 m. This is the depth range, where the contribution from both the BSBW and its "true" mode can be expected.

In general, the $\sigma_0 = 28.00$ kg m^{-3} in Figure 10b corresponds to the intermediate salinity minimum (centered at ~ 34.88) that is usually associated with the cooler and fresher BSBW inflow into the Nansen Basin. This salinity is within the range of the BSBW salinity in the SAT (34.7–34.9; Figures 4d–4f) [*Schauer et al.*, 2002a]. However, the temperature at the $\sigma_0 = 28.00$ kg m^{-3} is primarily above 0°C, which points to the importance of mixing and entrainment with the overlying warmer FSBW traced by the temperature maximum at ~ 200 m (Figure 10a). There are several events of decreasing temperature (by $\sim 0.5°C$) and salinity (by ~ 0.05) in the water layer between the σ_0 contours 28.00 and 28.04 kg m^{-3} (for example, periods I and III in Figures 10a and 10b) that are likely attributed to the pulses of the cooler and fresher BSBW from the SAT. In contrast, the warmer and saltier water event, which lasted 2.5 months from March to May 2007 (period II in Figure 10), is observed in the deeper layer (~ 1000–1800 m) between the σ_0 contours 28.02 and 28.06 kg m^{-3} that corresponds to the density range of the "true" mode of the BSBW in the SAT outflow. Overall, the entire period from December 2006 to June 2007 is characterized by relatively higher temperatures and salinities in 800–1800 m, the layer that is located significantly deeper than the core of the warm and saline FSBW boundary current at ~ 200 m (Figure 10a).

Expanding on our findings on the "true" mode of the BSBW in the SAT outflow, we suggest that the positive salinity and temperature anomaly in 800–1800 m is consistent with a pulse of the warmer and saltier "true" BSBW from the SAT. The seasonal timing of this pulse at M5 (March–May) is in agreement with the SAT mooring record showing seasonal appearance of the "true" BSBW in December-January. The CTD and temperature data from 420 and 510 m show that the BSBW does not contain the "true" BSBW fraction throughout the year. The near-bottom layer at 510 m shows significant variability, with temperature changing from 0.2°C in December 2009–January 2010 to $-1.3°C$ at the end of April (Figure 6a). We note, however, that the 1 year long records at the SAT and M5 moorings is not sufficient to build consistent conclusions on seasonal variability.

It is informative to compare the M5 time series with the cross-slope CTD observations reported by *Rudels et al.* [2013]. They found that in addition to the cold, less saline and dense BSBW that entered the boundary current below the warm FSBW core, a major fraction of the BSBW was following the 400 m isobaths on the upper slope of the northern Kara Sea as far as Severnaya Zemlya. This stream included a fairly saline upper mixed layer and a cold temperature maximum ($\sim 1°C$) overlying cold temperature and salinity minima and a more saline and warmer bottom layer similar to what has been observed at the eastern flank of the SAT in 1996 and in 2009–2010. This upper slope stream is not observed at the Laptev Sea slope and the strong reduction in temperature and salinity of the warm, saline core of the FSBW boundary current indicates that
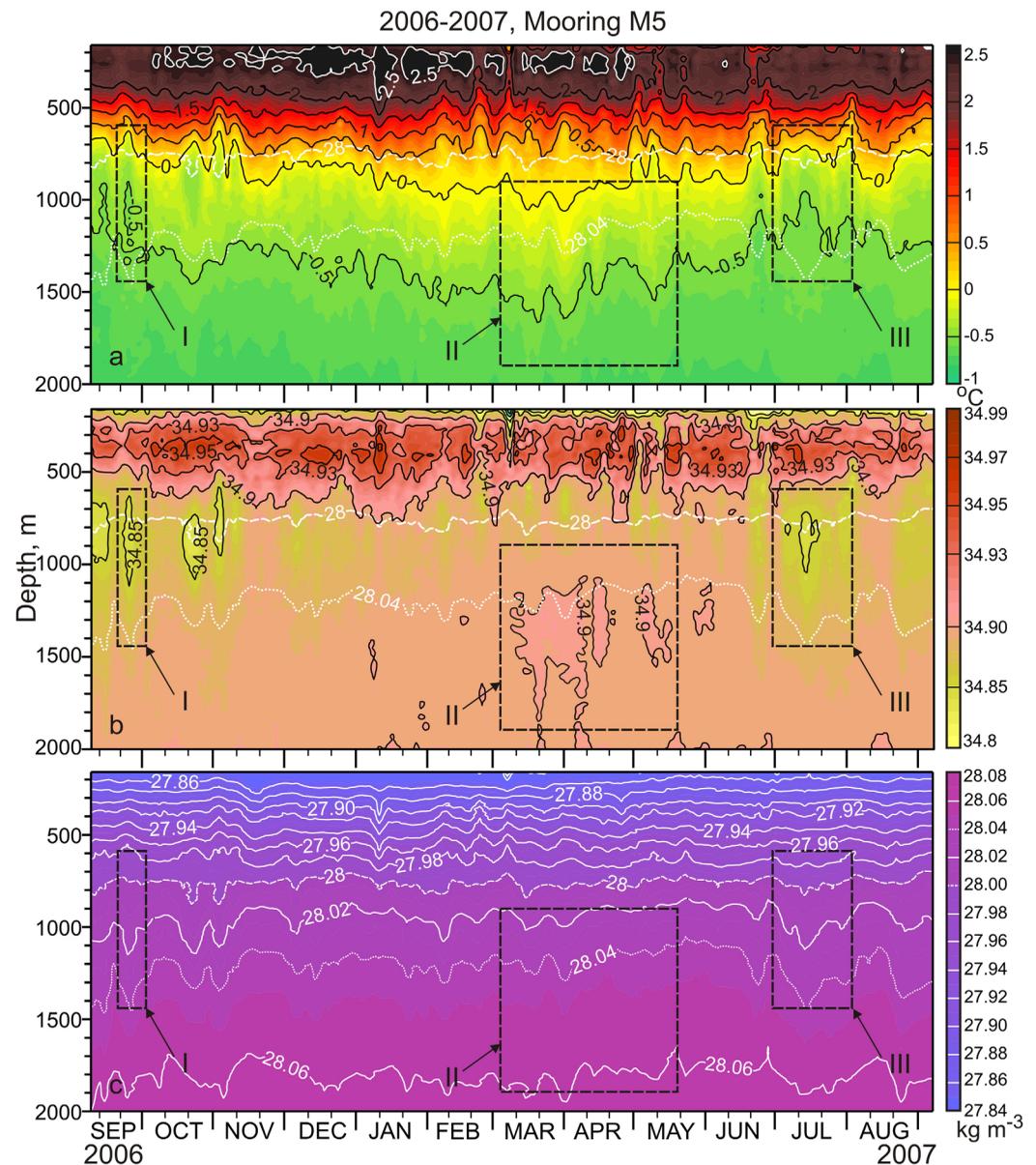
Figure 10. (a) Temperature (°C), (b) salinity, and (c) potential density (σ_0, kg m^{-3}) from the McLaine Moored Profiler (MMP) deployed off the Severnaya Zemlya continental slope at M5 mooring from 7 September 2006 to 7 September 2007. White dashed and dotted lines highlight σ_0 contours 28 and 28.04 kg m^{-3}, respectively. Black-dashed rectangular indicates (I and III) low-salinity/temperature events and (II) higher salinity/temperature events in 600–900 and 900–1900 m, respectively (see text for more explanations).

this fraction of the BSBW enters the boundary current and mixes with the FSBW. In this process the temperature of the descending BSBW increases by mixing with the warmer FSBW and the temperature minimum disappears, leaving only the salinity minimum to mark the core of the BSBW input [*Rudels et al.*, 2013, Figure 10].

The warm and saline pulse passing the mooring M5 northwest of the Laptev Sea in 2007, identified as a part of a more saline and warmer SAT outflow taking place at that time, also sheds light on the warm water mass located between 1000 and 1750 m depth above the 2000 m isobaths north of the Laptev Sea reported by *Rudels et al.* [2013] and interpreted as an eddy that just lost contact with the slope. Furthermore, since such warm and saline water was not observed west of Severnaya Zemlya, they assumed that this warmer eddy was created by dense boundary plumes from the Severnaya Zemlya shelf area, which had interacted with warm Atlantic Water. That interpretation is most likely wrong. The boundary plumes observed on the slope north of Severnaya Zemlya have been thin and attached to the bottom [*Rudels et al.*, 2000] and a thick

eddy is not likely to be created there, even if the Voronin Trough conceivably could channel dense water down the slope. A strong, persistent outflow like that in the SAT would be required. This eddy is shown together with a cold, low-salinity eddy observed in the intra basin in the central Lomonosov Ridge in *Rudels et al.* [2013, Figure 23]. The most plausible origin of the low-salinity eddy is the "true" mode of BSBW entering the Arctic Ocean in the SAT, and the difference between these two eddies indicates the range of the possible contributions supplied by the BSBW/SAT inflow.

The warmer "true" BSBW fraction of the SAT outflow shuts down completely in May–September 2010 (Figure 6a), pointing toward a possible seasonal variability that is also evident from M5 (Figure 10a) and was reported for the downstream locations in the central Laptev Sea [*Dmitrenko et al.*, 2006] and over the Siberian shelf junction with Lomonosov Ridge [*Dmitrenko et al.*, 2009b]. The increased fraction of the warmer and saltier "true" BSBW in the M5 mooring in December 2006 to June 2007 also corresponds to the decreased fraction of the cooler and fresher BSBW and vice versa in September–November 2006 and July–September 2008 (Figure 10). This is likely an indication of changing fractions of Atlantic Water in the total balance of the BSBW outflow from the SAT. Moreover, the gradual decrease in temperature at the bottom (510 m, Figure 6a) seems to be an indication that the input of brine-enriched water from the shallow area west of Novaya Zemlya suggested by *Schauer et al.* [2002a] and *Rudels et al.* [2013] to provide the densest outflow from the Barents and Kara Seas is increasing in strength during the winter and is gradually cooling and freshening the warmer Atlantic Water, changing the characteristics observed at mooring M5.

A single CTD profile taken in the trough in 2010 (Figure 9) also indicates a salinity minimum and cold but slightly higher salinity at the bottom. This would suggest that the Barents Sea and the SAT outflow could provide both the deep temperature minimum and the high-salinity bottom water observed in the Eurasian Basin. This would be an alternative to the suggestion by *Rudels et al.* [2000] that the densest water could be formed by brine rejection around Severnaya Zemlya but the temperature minimum had to be provided by the SAT outflow because it would then avoid entrainment of warm Atlantic and intermediate water.

4.3. SAT Flow Based on Year-Long Mooring Record

In this section we assess the temperature, salinity, and σ_0 year-long records from the SAT mooring. We show that an important portion of temperature and salinity variability at the SAT mooring is associated with temporal variability in the density of the water flowing into the Arctic Ocean through the SAT. This results in a vertical displacement of the isopycnals relative to the fixed-depth level of CTD observations.

The water column at the SAT eastern flank shows at least three distinct water masses each with a different fraction of Atlantic Water: the SAT-circulating FSBW, BSBW and "true" mode of the BSBW. Among these three, the SAT-circulating FSBW and "true" BSBW contain a relatively high fraction of warm and saline Atlantic Water comprising two intermediate maximums in temperature and salinity on the *TS* plane (Figures 2 and 9). These maximums are also evident in temperature and salinity vertical distributions (Figures 3 and 4). The σ_0 shows gradual increase with depth indicating that all temperature and salinity anomalies are density-compensating (Figure 6c). Thus, vertical water mass displacements in the eastern SAT are likely to result in coherent σ_0 changes throughout the water column. In contrast, the associated changes in temperature and salinity are expected to be uncorrelated with σ_0, due to the differences in temperature and salinity of the three water masses present. This is in agreement with the mooring time series shown in Figure 6. Furthermore, because the maxima/minima of salinity and temperature for the FSBW, BSBW and "true" mode of the BSBW are separated by 15–80 m, the salinity and temperature time series at the fixed-depth levels can exhibit pure correlation that is consistent with mooring observations (Figure 6).

In the following we test the stability of the water mass structure by exploring the *TS* scatterplot compiled based on all available temperature and salinity records from the SAT mooring (Figure 9). While the temporal variability of temperature and salinity is significant, the structure in the *TS* plane is maintained throughout the entire period of mooring observations. Moreover, the core of the FSBW, BSBW and "true" BSBW defined by corresponding temperature and salinity extremes match nearly the same σ_0 level of 27.93, 28.00, and 28.07 kg m^{-3}, respectively, Figure 9a (note that data from 420 m are insufficient to build consistent conclusions about the "true" BSBW). For example, during period II the BSBW is warmer and saltier compared with period III (Figures 9d and 9e). However, the BSBW core maintains a similar σ_0 defining the knee in the *TS* plane at ∼28.00 kg m^{-3} (Figures 9d and 9e).

Overall, the *T*, *S*, and σ_0 vertical distribution allows suggesting that incoherent temporal changes in temperature and salinity in Figure 6 are conditioned by vertical displacement of the water masses relative to the
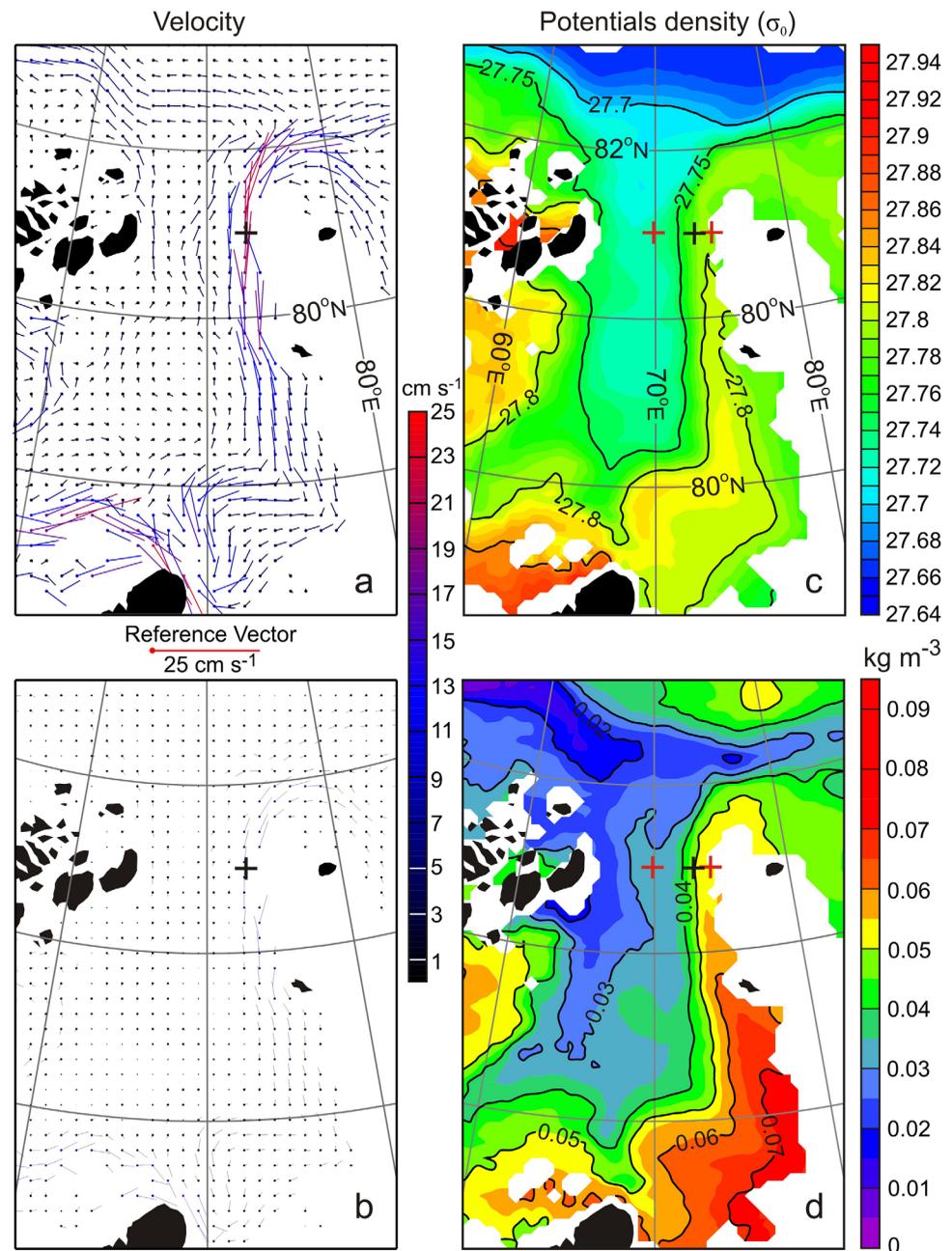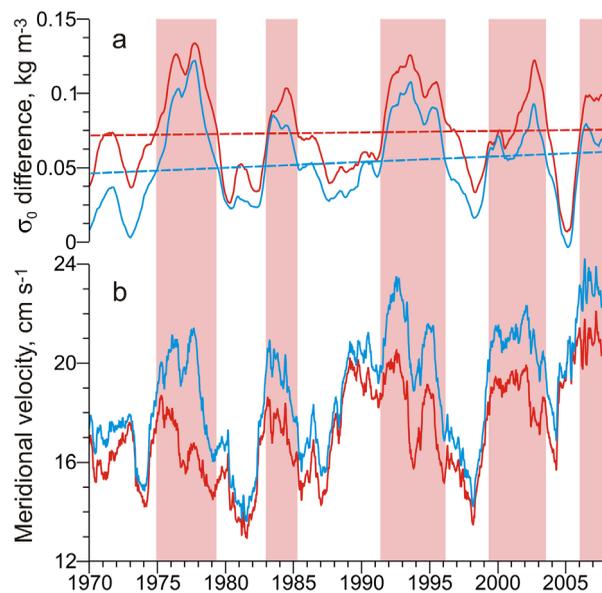
Figure 11. Simulated (left) velocity and (right) potential density (σ_0) at 150 m for (top) the long-term mean (1970–200 7) and (bottom) the mean difference between events with positive and negative velocity anomalies defined by $\pm$one standard deviation of the mean along-trough velocity at the mooring position marked with black cross. Red crosses show the grid nods where the σ_0 is taken to calculate the cross-slope σ_0 difference shown in Figure 12a.

fixed-depth levels of CTD observations. The role of advection in modifying the *TS* properties of the principal water mass is evident (Figures 9 and 10). In the following, however, we focus on the potential density variations assuming their role in conditioning the SAT flow to the Arctic Ocean.

4.4. Dynamics of the Atlantic Water Flow to the Arctic Ocean Through the SAT

During period II–III, mooring data shows simultaneous increase of density at 140–260 m accompanied by slowing of the SAT flow to the Arctic Ocean superimposed onto synoptic variability (Figures 6c and 8). We speculate that the density increase at mooring location is conditioned by weakening of the density gradient

across the SAT eastern slope. Hypothetically this results in weaker thermohaline forcing and a corresponding slowing of the SAT flow to the Arctic Ocean. In this scenario, the background synoptic variability seen in Figure 8 is likely driven by the atmospheric forcing as reported by *Kirillov et al.* [2012]. Overall, the barotropic events of increased velocities in periods I–III (Figure 8) are consistent with the findings of *Lien et al.* [2013]. They show that wind-forced transient increases in the flow through the Barents Sea on time scales of days to weeks are identifiable also downstream along the eastern flank of the SAT.

Indeed, our mooring record at single location is not properly resolving spatial variability across the SAT. Hence, we involve numerical simulations to reveal patterns of the SAT flow, particularly the relationship between velocity and cross-trough density gradient. The NEMO model simulates well oceanographic conditions in the SAT. The simulated long-term mean (1970–2007)

Figure 12. (a) The simulated potential density difference (kg m^{-3}) across the SAT eastern slope along 81°N and (b) the simulated along-trough velocity (cm s^{-1}) at the SAT mooring for (red) 150 m and (blue) 300 m. The original 5 day mean data were smoothed by 1 year running mean. Pink shading depicts the positive anomaly of the σ_0 difference relative to the linear trend shown in Figure 12a by dashed lines.

density field across the SAT is qualitatively consistent with that sampled in 2008–2010 (Figure 5). At 150 m the long-term mean (1970–2007) obtained from averaging 5 day means shows the jet of the SAT outflow following the eastern flank with the mean northward velocity ~17 cm s^{-1} at position of the SAT mooring (Figures 11a and 12b). This is quantitatively consistent with the 1 year mean 17 cm s^{-1} measured by the moored ADCP at 150 m (Figure 7a). The cross-slope σ_0 difference at 150 m (between red crosses in Figure 11c) of ~0.07 kg m^{-3} (Figures 5d, 11c, and 12a) realistically represents that for the 2008 and 2009 (Figures 5a and 5b). The simulated circulation patterns in the SAT are almost identical to those derived by *Panteleev et al.* [2007] using a variational data assimilation technique.

For evaluating the role of thermohaline forcing of the SAT flow, we compile the mean velocity and σ_0 difference (Figures 11b and 11d, respectively) between velocity events with positive and negative anomalies defined as exceeding the mean along-trough velocity at the SAT mooring (17 cm s^{-1}) by $\pm$ one standard deviation (7 cm s^{-1}). The positive anomaly of the SAT flow is spatially coherent along the SAT eastern flank and further downstream over the Kara Sea continental margin (Figure 11b). In contrast, the western flank shows smaller changes associated with enhanced outflow. It is also evident that the positive anomaly of the SAT outflow is accompanied by increasing the cross-slope σ_0 difference from ~0.025 kg m^{-3} at the SAT mooring to ~0.035 kg m^{-3} at the Kara Sea continental slope. This is in line with simulated time series (1970–2007) of the cross-slope σ_0 difference and SAT outflow at mooring location showing coherent changes in σ_0 cross-slope difference and along-trough velocity for the depth of the SAT-circulating FSBW (150 m, red) and BSBW (300 m, blue) with an apparent increase of the baroclinic component with increasing σ_0 difference (Figure 12). Overall, this suggests that the mean SAT outflow velocity of 17 $\pm$ 7 cm s^{-1} is subject to the density-driven temporal variability caused by spatial variability in cross-slope σ_0 distribution. Such variability could arise from the different travel times of the BSBW and the FSBW from their separation in the Norwegian Sea to their confluence in the northern Kara Sea and subsequent out-of-phase responses to temporal variability in hydrographic properties of the Atlantic Water flow toward the Arctic [e.g., *Dmitrenko et al.*, 2009b]. In addition, the modification of the BSBW while en route, varies due to corresponding changes in the response within the Barents Sea to Atlantic Water anomalies, such as e.g., reduced sea-ice cover [e.g., *Årthun et al.*, 2012]. Indeed, both the modeled velocity and density difference (Figure 12) vary in phase with the reported salinity anomaly of the 1970s [*Dickson et al.*, 1988], the salinity anomaly in the 1980s [*Belkin et al.*, 1998], as well as the salinity anomaly of the 1990s [*Belkin*, 2004]. Hence, our model results are consistent with the findings of *Smedsrud*

et al. [2013], who based on a climate model simulation reported a positive relation between changes in the inflow to the Barents Sea, the density of the BSBW, and subsequently the volume transport of the BSBW through the northern Kara Sea.

The cross-slope σ_0 gradient is controlled by complex interaction between the FSBW and BSBW. In fact, during period III the denser water in 140–260 m was conditioned by significant cooling that was not fully compensated in the density field by simultaneous freshening (e.g., Figure 9e). This indicates a lower fraction of the warm and saline Atlantic Water inflow to SAT with FSBW and/or more intense vertical mixing with BSBW accompanied by intensive heat loss. The role of water masses interaction in forming the cross-slope density gradient is outside the scope of this paper. We limit our discussion in this direction to only suggesting that the appearance of the baroclinic current component forced by an increased cross-slope σ_0 gradient can contribute to shear-driven instability at the upper boundary of the FSBW [*Dmitrenko et al.*, 2014]. In turn, this results in enhanced heat loss from the FSBW with possible implication for the sea-ice cover during periods with increased σ_0 gradient.

5. Summary and Conclusive Remarks

This paper addresses the issue of water mass attribution in the SAT with special focus on the Atlantic Water flowing to the Arctic Ocean through the SAT.

Our findings show that the water column above the eastern slope of the SAT comprises three different water masses of Atlantic origin. The intrusion of the cooler and fresher BSBW into the merged Atlantic Water branches downstream the SAT mouth has been suggested to maintain the knee in the *TS* plane at $\sigma_0 = 27.97$–28.03 kg m^{-3} [e.g., *Rudels et al.*, 2000; *Woodgate et al.*, 2001; *McLaughlin et al.*, 2002; *Dmitrenko et al.*, 2008, 2009a]. This was also reported from the SAT eastern flank by *Schauer et al.* [2002a, 2002b]. However, contrary to the view that salinity and temperature increase below the BSBW toward the bottom is an effect of pure shelf/slope convection [*Rudels et al.*, 2000; *Schauer et al.*, 2002b], we explain this warmer and saltier bottom layer as BSBW consisting of a relatively higher fraction of Atlantic Water. We therefore refer to this water mass as the "true" mode of the BSBW. In fact, the "true" mode of the BSBW constitutes a core of Atlantic origin within the BSBW.

Furthermore, we find evidence that a fraction of the saltier and warmer "true" BSBW remains recognizable downstream of the SAT along the Siberian continental margin over the density range $28.02 < \sigma_0 < 28.06$ kg m^{-3}, which corresponds to the depth range $\sim$900–1800 m (Figure 10). Hence, our results clearly show that the "true" mode of the BSBW can supply relatively warm and saline water of Atlantic origin to the deeper Arctic Ocean, leading to a warmer and saltier Arctic Ocean between 900 and 1800 m, where the changes in the thermohaline structure are supposed to be very conservative. Thus, our findings support the hypothesis proposed by *Aagaard and Woodgate* [2001] that less entrainment of meltwater into the BSBW will lead to a warmer, more saline and denser BSBW core, which penetrates deeper into the Arctic Ocean water column.

In addition, we have presented observational evidence of a strong outflow of 17–22 cm s^{-1} from the Kara Sea to the Arctic Ocean along the SAT eastern flank that is in agreement with model simulations. Our results indicate that this current is in geostrophic balance and can be partially maintained by the density gradient across the eastern flank of the SAT. Similar results are also seen in numerical model simulations. The stronger velocity and coherence with density gradient in the deeper layer (300 m) is consistent with a bottom intensified, baroclinic current component [*Schauer et al.*, 2002a; *Gammelsrød et al.*, 2009] in the SAT outflow. Our observational data and model simulations clearly show barotropic responses on time scales of days to weeks and baroclinic responses to changes in the cross-slope density gradient on time scales of months to years (Figures 6c, 8, and 12). These findings support the conclusions by *Lien et al.* [2013] and *Kirillov et al.* [2012] with regard to a barotropic response of the SAT outflow to atmospheric circulation, and the findings of *Smedsrud et al.* [2013] showing a baroclinic response in the SAT outflow to inter-annual density variations in the BSBW.

Our analysis was limited by the availability of velocity and CTD data from a single location only. The deficiencies of the conducted analyses clearly define a necessity for further research in this area. A more extensive and representative mooring array crossing the SAT is needed in order to empirically investigate our findings derived from the model simulations, including a proper estimation of SAT volume and heat

transports. Moreover, further modeling efforts are necessary to investigate hydrodynamic instability and eddy generation caused by the interaction between the SAT outflow and the Arctic Ocean FSBW boundary current.

References

Aagaard, K., and R. A. Woodgate (2001), Some thoughts on the freezing and melting of sea ice and their effects on the ocean, *Ocean Model.*, *3*, 127–135.

Aksenov, Y., S. Bacon, A. Coward, and A. J. G. Nurser (2010), The North Atlantic inflow to the Arctic Ocean: High-resolution model study, *J. Mar. Syst.*, *79*, 1–22, doi:10.1016/j.jmarsys.2009.05.003.

Aksenov, Y., V. Ivanov, G. Nurser, S. Bacon, I. Polyakov, A. Coward, A. Naveira-Garabato, and A. Beszczynska-Möller (2011), The Arctic circumpolar boundary current, *J. Geophys. Res.*, *116*, C09017, doi:10.1029/2010JC006637.

Arakawa, A. (1966), Computational design of long-term numerical integration of the equations of fluid motion, *J. Comput. Phys.*, *1*, 119–143.

Årthun, M., and C. Schrum (2010), Ocean surface heat flux variability in the Barents Sea, *J. Mar. Syst.*, *83*, 88–98.

Årthun, M., R. B. Ingvaldsen, L. H. Smedsrud, and C. Schrum (2011), Dense water formation and circulation in the Barents Sea, *Deep Sea Res., Part I*, *58*, 801–817, doi:10.1016/j.dsr.2011.06.001.

Årthun, M., T. Eldevik, L. H. Smedsrud, Ø. Skagseth, and R. B. Ingvaldsen (2012), Quantifying the influence of Atlantic heat on Barents Sea ice variability and retreat, *J. Clim.*, *25*, 4736–4743, doi:10.1175/JCLI-D-11-00466.1.

Barnier, B., et al. (2006), Impact of partial steps and momentum advection schemes in a global ocean circulation model at eddy permitting resolution, *Ocean Dyn.*, *56*, 543–567.

Belkin, I. M. (2004), Propagation of the "Great Salinity Anomaly" of the 1990s around the northern North Atlantic, *Geophys. Res. Lett.*, *31*, L08306, doi:10.1029/2003GL019334.

Belkin, I. M., S. Levitus, J. Antonov, and S. Malmberg (1998), "Great salinity anomalies" in the North Atlantic, *Prog. Oceanogr.*, *41*, 1–68.

Beszczynzka-Möller, A., E. Fahrbach, U. Schauer, and E. Hansen (2012), Variability in Atlantic water temperature and transport at the entrance to the Arctic Ocean, 1997–2010, *ICES J. Mar. Sci.*, *69*(5), 852–863, doi:10.1093/icesjms/fss056.

Blindheim, J. (1989), Cascading of Barents Sea bottom water into the Norwegian Sea, *Rapp. P. V. Réun. Cons. Int. Explor. Mer.*, *188*, 49–58.

Dai, A., and K. E. Trenberth (2002), Estimates of freshwater discharge from continents: Latitudinal and seasonal variations, *J. Hydrometeorol.*, *3*, 660–687.

Defant, A. (1961), *Physical Oceanography*, vol. 1, 729 pp., Pergamon, N. Y.

Dickson, R. R., J. Meincke, S. A. Malmberg, and A. J. Lee (1988), The great salinity anomaly in the Northern North-Atlantic 1968–1982, *Prog. Oceanogr.*, *20*(2), 103–151.

Dmitrenko, I., I. Polyakov, S. Kirillov, L. Timokhov, H. Simmons, V. Ivanov, and D. Walsh (2006), Seasonal variability of Atlantic water on the continental slope of the Laptev Sea during 2002–2004, *Earth Planet. Sci. Lett.*, *244*(3–4), 735–743, doi:10.1016/j.epsl.2006.01.067.

Dmitrenko, I. A., S. A. Kirillov, V. V. Ivanov, and R. A. Woodgate (2008), Mesoscale Atlantic water eddy off the Laptev Sea continental slope carries the signature of upstream interaction, *J. Geophys. Res.*, *113*, C07005, doi:10.1029/2007JC004491.

Dmitrenko, I. A., D. Bauch, S. A. Kirillov, N. Koldunov, P. J. Minnett, V. V. Ivanov, J. A. Hölemann, and L. A. Timokhov (2009a), Barents Sea upstream events impact the properties of Atlantic water inflow into the Arctic Ocean: Evidence from 2005–2006 downstream observations, *Deep Sea Res., Part I*, *56*(4), 513–527, doi:10.1016/j.dsr.2008.11.005.

Dmitrenko, I. A., et al. (2009b), Seasonal modification of the Arctic Ocean intermediate water layer off the eastern Laptev Sea continental shelf break, *J. Geophys. Res.*, *114*, C06010, doi:10.1029/2008JC005229.

Dmitrenko, I. A., et al. (2014), Heat loss from the Atlantic water layer in the northern Kara Sea: Causes and consequences, *Ocean Sci.*, *10*, 719–730, doi:10.5194/os-10-719-2014.

Ellingsen, I., D. Slagstad, and A. Sundfjord (2009), Modification of water masses in the Barents Sea and its coupling to ice dynamics: A model study, *Ocean Dyn.*, *59*, 1095–1108, doi:10.1007/s10236-009-0230-5.

Fichefet, T., and M. A. Morales Maqueda (1997), Sensitivity of a global sea ice model to the treatment of ice thermodynamics and dynamics, *J. Geophys. Res.*, *102*, 12,609–12,646.

Furevik, T. (2001), Annual and interannual variability of Atlantic water temperatures in the Norwegian and Barents Seas: 1980–1996, *Deep Sea Res., Part I*, *48*, 383–404.

Gammelsrød, T., Ø. Leikvin, V. Lien, W. P. Budgell, H. Loeng, and W. Maslowski (2009), Mass and heat transports in the NE Barents Sea: Observations and models, *J. Mar. Syst.*, *75*, 56–69.

Hanzlick, D., and K. Aagaard (1980), Freshwater and Atlantic water in the Kara Sea, *J. Geophys. Res.*, *85*, 4937–4942.

Ingvaldsen, R., L. Asplin, and H. Loeng (2004), The seasonal cycle in the Atlantic transport to the Barents Sea during the years 1997–2001, *Cont. Shelf Res.*, *24*, 1015–1032.

Ivanov, V. V., V. A. Alexeev, I. Repina, N. V. Koldunov, and A. Smirnov (2012), Tracing Atlantic water signature in the Arctic Sea ice cover East of Svalbard, *Adv. Meteorol.*, doi:10.1155/2012/201818.

Jahn, A., et al. (2012), Arctic Ocean freshwater budget—How robust are model simulations?, *J. Geophys. Res.*, *117*, C00D16, doi:10.1029/2012JC007907.

Johnson, M., et al. (2012), Evaluation of Arctic sea ice thickness simulated by AOMIP models, *J. Geophys. Res.*, *117*, C00D13, doi:10.1029/2011JC007257.

Kirillov, S. A., I. A. Dmitrenko, V. V. Ivanov, E. O. Aksenov, M. S. Makhotin, and B. A. de Quevasb (2012), The influence of atmospheric circulation on the dynamics of the intermediate water layer in the eastern part of the St. Anna Trough, *Dokl. Earth Sci.*, *444*(1), 630–633, doi:10.1134/S1028334X12050121.

Knipovitch, N. (1905), Hydrologische Untersuchungen im Europäischen Eismeer, Annalen der Hydrographie und Maritimen Meteorologie, Sonderabdruck, 62 p.

Levitus, S., T. P. Boyer, M. E. Conkright, T. O'Brien, J. Antonov, C. Stephens, L. Stathoplos, D. Johnson, and R. Gelfeld (1998a), Volume 1: Introduction, in *NOAA Atlas NESDIS 18, World Ocean Database 1998*, U.S. Gov. Print. Off., Washington, D. C.

Levitus, S., T. P. Boyer, M. E. Conkright, D. Johnson, T. O'Brien, J. Antonov, C. Stephens, and R. Gelfeld (1998b), Volume 2: Temporal distribution of mechanical bathythermograph profiles, in *NOAA Atlas NESDIS 19, World Ocean Database 1998*, U.S. Gov. Print. Off., Washington, D. C.

Lien, V. S., and A. G. Trofimov (2013), Formation of Barents Sea branch water in the northeastern Barents Sea, *Polar Res.*, *32*, 18905, doi:10.3402/polar.v32i0.18905.

Lien, V. S., F. Vikebø, and Ø. Skagseth (2013), One mechanism contributing to co-variability of the Atlantic inflow branches to the Arctic, *Nat. Commun.*, *4*, 1488.

Lique, C., A. M. Treguier, M. Scheinert, and T. Penduff (2009), A model-based study of ice and freshwater transport variability along both sides of Greenland, *Clim. Dyn.*, *33*(5), 685–705, doi:10.1007/s00382-008-0510-7.

Lique, C., A. M. Treguier, B. Blanke, and N. Grima (2010), On the origins of water masses exported along both sides of Greenland: A Lagrangian model analysis, *J. Geophys. Res.*, *115*, C05019, doi:10.1029/2009JC005316.

Loeng, H., V. Ozhigin, and B. Ådlandsvik (1997), Water fluxes through the Barents Sea, ICES, *J. Mar. Sci.*, *54*, 310–317.

Madec, G., and NEMO Team (2008), NEMO Ocean Engine, version 3.2, in *Note du Pole de modelisation*, 27, Inst. Pierre-Simon Laplace.

Marsh, R., D. Desbruyères, J. L. Bamber, B. A. de Cuevas, A. C. Coward, and Y. Aksenov (2010), Short-term impacts of enhanced Greenland freshwater fluxes in an eddy-permitting ocean model, *Ocean Sci.*, *6*, 749–760.

Martin, S., and D. J. Cavalieri (1989), Contributions of the Siberian shelf polynyas to the Arctic Ocean intermediate and deep water, *J. Geophys. Res.*, *94*, 12,725–12,738.

McLaughlin, F. A., E. C. Carmack, R. W. Macdonald, A. Weaver, and J. N. Smith (2002), The Canada Basin 1989–1995: Upstream events and far-field effects of the Barents Sea, *J. Geophys. Res.*, *107*(C7), 3082, doi:10.1029/2001JC000904.

Midttun, L. (1985), Formation of dense bottom water in the Barents Sea, *Deep Sea Res., Part A*, *32*, 1233–1241.

Nansen, F. (1902), Oceanography of the North Polar Basin, in *The Norwegian North Polar Expedition 1893–1896: Scientific Results*, vol. 3, no. 9, 427 pp.

Nansen, F. (1906), Northern waters, in *Captain Roald Amundsen's Oceanographic Observations in the Arctic Seas in 1901*, vol. 1, no. 3, 145 pp., Vid-selskap Skrifter I, Mat.-Naturv. kl. Dybvad Christiania.

Onarheim, I. H., L. H. Smedsrud, R. B. Ingvaldsen, and F. Nilsen (2014), Loss of sea ice during winter north of Svalbard, *Tellus, Ser. A, 66*, 23933.

Panteleev, G., A. Proshutinsky, M. Kulakov, D. A. Nechaev, and W. Maslowski (2007), Investigation of the summer Kara Sea circulation employing a variational data assimilation technique, *J. Geophys. Res.*, *112*, C04S15, doi:10.1029/2006JC003728.

Petermann, A. (1865), *Der Nordpol und Südpol, die Wichtigkeit ihrer Erforschung in Geographischer und Kulturhistorischer Beziehung*, pp. 146–160, Mit Bemerkungen über die Strömungen der Polar-Meere. Pet. Mitt., Gotha.

Popova, E. E., A. Yool, A. C. Coward, Y. K. Aksenov, S. G. Alderson, B. A. de Cuevas, and T. R. Anderson (2010), Control of primary production in the Arctic by nutrients and light: Insights from a high resolution ocean general circulation model, *Biogeoscience*, *7*(11), 3569–3591.

Popova, E. E., A. Yool, Y. Aksenov, and A. C. Coward (2013), Role of advection in Arctic Ocean lower trophic dynamics: A modeling perspective, *J. Geophys. Res. Oceans*, *118*, 1571–1586, doi:10.1002/jgrc.20126.

Quadfasel, D., B. Rudels, and S. Selchow (1992), The Central Bank vortex in the Barents Sea: Water mass transformation and circulation, *ICES Mar. Sci. Symp.*, *195*, 40–51.

Rudels, B. (2001), Ocean current: Arctic basin circulation, in *Encyclopaedia of Ocean Sciences*, edited by J. Steele, S. Thorpe, and K. Turekian, pp. 177–187, Academic.

Rudels, B. (2010), Constraints on exchanges in the Arctic Mediterranean: Do they exist and can they be of use?, *Tellus, Ser. A*, *62*, 109–122.

Rudels, B. (2012), Arctic Ocean circulation and variability–advection and external forcing encounter constraints and local processes, *Ocean Sci.*, *8*, 261–286, doi:10.5194/os-8-261-2012.

Rudels, B., and H. J. Friedrich (2000), The transformations of Atlantic water in the Arctic Ocean and their significance for the freshwater budget, in *The Freshwater Budget of the Arctic Ocean, NATO Sci. Ser. 2. Environ. Security*, vol. 70, edited by E. L. Lewis et al., pp. 503–532, Kluwer Acad., Dordrecht, Netherlands.

Rudels, B., E. P. Jones, L. G. Anderson, and G. Kattner (1994), On the intermediate depth waters of the Arctic Ocean, in *The Polar Oceans and Their Role in Shaping the Global Environment: The Nansen Centennial Volume, Geophys. Monogr. Ser.*, vol. 84985, edited by O. M. Johannessen, R. D. Muench, and J. E. Overland, pp. 33–46, AGU, Washington, D. C.

Rudels, B., R. D. Muench, J. Gunn, U. Schauer, and H. J. Friedrich (2000), Evolution of the Arctic Ocean boundary current north of the Siberian shelves, *J. Mar. Syst.*, *25*, 77–99.

Rudels, B., P. E. Jones, U. Schauer, and P. Eriksson (2004), Atlantic sources of the Arctic Ocean surface and halocline waters, *Polar Res.*, *23*(2), 181–208.

Rudels, B., U. Schauer, G. Björk, M. Korhonen, S. Pisarev, B. Rabe, and A. Wisotzki (2013), Observations of water masses and circulation with focus on the Eurasian Basin of the Arctic Ocean from the 1990s to the late 2000s, *Ocean Sci.*, *9*, 147–169.

Rudels, B., M. Korhonen, U. Schauer, S. Pisarev, B. Rabe, and A. Wisotzki (2015), Circulation and transformation of Atlantic water in the Eurasian Basin and the contribution of the Fram Strait inflow branch to the Arctic Ocean heat budget, *Prog. Oceanogr.*, *132*, 128–152, doi:10.10167j.pocean.2014.04.003.

Schauer, U., R. D. Muench, B. Rudels, and L. Timokhov (1997), Impact of eastern Arctic shelf waters on the Nansen Basin intermediate layers, *J. Geophys. Res.*, *102*, 3371–3382.

Schauer, U., H. Loeng, B. Rudels, V. K. Ozhigin, and W. Dieck (2002a), Atlantic water flow through the Barents and Kara Seas, *Deep Sea Res., Part I*, *49*(12), 2281–2298.

Schauer, U., B. Rudels, E. P. Jones, L. G. Anderson, R. D. Muench, G. Björk, J. H. Swift, V. Ivanov, and A. M. Larsson (2002b), Confluence and redistribution of Atlantic water in the Nansen, Amundsen and Makarov basins, *Ann. Geophys.*, *20*(2), 257–273.

Skagseth, Ø., T. Furevik, R. Ingvaldsen, H. Loeng, K. A. Mork, K. A. Orvik, and V. Ozhigin (2008), Volume and heat transports to the Arctic Ocean via the Norwegian and Barents Seas, in *Arctic-Subarctic Ocean Fluxes: Defining the Role of the Northern Seas in Climate*, edited by R. R. Dickson, J. Meincke, and P. Rhines, pp. 45–64, Springer, Netherlands.

Smedsrud, L. H., R. Ingvaldsen, J. E. Ø. Nilsen, and Ø. Skagseth (2010), Heat in the Barents Sea: Transport, storage, and surface fluxes, *Ocean Sci.*, *6*, 219–234.

Smedsrud, L. H., et al. (2013), The role of the Barents Sea in the Arctic climate system, *Rev. Geophys.*, *51*, 415–449, doi:10.1002/rog.20017.

Steele, M., J. H. Morison, and T. B. Curtin (1995), Halocline water formation in the Barents Sea, *J. Geophys. Res.*, *100*, 881–894.

Steele, M., R. Morley, and W. Ermold (2001), PHC: A global hydrography with a high quality Arctic Ocean, *J. Clim.*, *14*(9), 2079–2087.

Tsubouchi, T., S. Bacon, A. C. Naveira Garabato, Y. Aksenov, S. Laxon, E. Fahrbach, A. Beszczynska-Möller, E. Hansen, C. Lee, and R. Ingvaldsen (2012), The Arctic Ocean in summer: Boundary fluxes and water mass transformation, *J. Geophys. Res.*, *117*, C01024, doi:10.1029/2011JC007174.

van Campen, S. R. (1876), *The Dutch in the Arctic Seas*, 263 p., Truübner, London, U. K.

Woodgate, R. A., K. Aagaard, R. D. Muench, J. Gunn, G. Bjork, B. Rudels, A. T. Roach, and U. Schauer (2001), The Arctic Ocean boundary current along the Eurasian slope and the adjacent Lomonosov Ridge: Water mass properties, transports and transformations from moored instruments, *Deep Sea Res., Part I*, *48*, 1757–1792.